UiO : Department of Geosciences
University of Oslo

Ice Nucleating Particles in Arctic Clouds and Their Impact on Climate

Astrid Bragstad Gjelsvik

Master's Thesis, Spring 2022

Abstract

Projections of global climate change and Arctic amplification are sensitive to the representation of low-level cloud phase in models, which constitutes an important model uncertainty. Ice nucleating particles (INPs) are necessary for primary ice formation in clouds at temperatures above approximately -38°C, and can therefore be important for cloud phase and the radiative effect of clouds. Knowledge of these INPs is limited, especially in remote regions such as the Arctic. In this thesis, observations of INPs acting in the immersion mode were carried out at Andenes, Norway, during cold air outbreaks in March 2021. The INP concentrations were quantified using the home-built DRoplet Ice Nuclei Counter Oslo. The observations show that the INP concentration was uncorrelated with aerosols of diameter ≥ 0.5 μm and the total organic carbon in the adjacent sea water, used as a proxy for a potential INP source. Based on this nature of the INP concentrations, the INP observations were used as a basis for a new and purely temperature-dependent parameterisation of immersion freezing INPs for the Arctic and implemented into the Norwegian Earth System Model. The implementation of the parameterisation results in an average increase in cloud liquid water path of 9.2 g/m^2 for the Arctic in the present climate, and significantly improves the supercooled liquid fractions for each cloud isotherm, compared to CALIOP LiDAR observations from Space. The change in cloud liquid water path is found to likely be the dominant contributor to the simulated average increase in net cloud radiative effect at the surface of 2 W/m^2. This results in a lower limit estimate of an average surface temperature increase of 0.3°C in the Arctic, with a seasonal maximum of 0.7°C in boreal autumn. These findings indicate that INPs could have a significant impact on Arctic clouds and radiation, and that further research on INPs is important to determine their effect in a changing climate.

Samandrag

Prognosane for global oppvarming og den særskild forsterka oppvarminga i Arktis er ømfintlege for korleis klimamodellar representerer fasen til låge skyer. Dette utgjer ei uvisse for modellane. For at is skal dannast i atmosfæren ved temperaturar høgare enn om lag -38°C og utan annan is til stades, er nærværet av visse partiklar naudsynt. Vi kallar desse partiklane for iskjernedannande partiklar (IKP-ar), og dei kan spele ei viktig rolle for fasen til skyene og strålingspåverknaden deira. Kunnskapen om desse IKP-ane er avgrensa, særskild i avsidesliggande område som Arktis. I denne oppgåva har vi gjort observasjonar av IKP-ar som dannar is medan dei er innkapsla i vassdropar, i mars 2021 ved Andenes i Noreg. Vi gjorde målingane samstundes som utbrot av polare luftmassar nådde observasjonsstaden vår, og nytta det heimebygde instrumentet DRoplet Ice Nuclei Counter Oslo. Vi fann ikkje nokon korrelasjon mellom IKP-konsentrasjonane og aerosolar med storleik ≥ 0.5 μm, eller med konsentrasjonen av det totale organiske karbonet i det nærliggande havvatnet. Den sistnemnde storleiken undersøkte vi som representant for ei mogleg kjelde til IKP-ar frå havet. Med grunnlag i karakteren til desse IKP-ane, laga vi ei ny parameterisering for innkapsla IKP-ar i Arktis som berre var bunden av temperatur, og implementerte ho i klimamodellen Norwegian Earth System Model. Denne implementeringa førte til ei gjennomsnittleg auking i vatninnhaldet i skyene i heile luftkolonnen på 9.2 g/m^2 i Arktis i noverande klima. Ho førte òg til at delen med underkjølt vatn for kvar isoterm i skyene betra seg, samanlikna med verdsromobservasjonar frå CALIOP-LiDAR-en. Vi fann at denne endringa i vatninnhaldet i skyene kunne forklare mykje av den gjennomsnittlege aukinga i den samanlagte strålingspåverknaden til skyene ved jordoverflata på 2 W/m^2 i simuleringa. Denne aukinga førte til ei gjennomsnittleg temperaturauking ved overflata på minst 0.3°C i Arktis, med eit høgdepunkt på 0.7°C på hausten (nordleg halvkule). Desse funna gjev grunn til å tru at IKP-ar kan ha ein monaleg påverknad på skyer og stråling i Arktis, og at meir forsking på IKP-ar er viktig for å vite kva rolle dei kjem til å spele i eit klima i endring.

Acknowledgements

My supervisors Rob David and Trude Storelvmo have been a rock'n'roll duo during the writing of this thesis. Thank you for all your valuable insight and knowledge that has gone into this thesis and lifted it, as well as your encouragement and interest. I am grateful for all the time you have set aside for discussions with me, whether they have been of academic or more existential nature. Many thanks also to Stefan Hofer and Zachary McGraw for helping me with the technicalities of climate modelling, and for your very much appreciated input. Thank you to Tim Carlsen and Franziska Hellmuth for giving me advice and help along the way, as well as being an incredible campaign crew together with Rob and Britta Schäfer, and master students Ingrid and Stian. You all, as well as the researchers from ISLAS, made the campaign in Andenes a truly privileged and educational experience.

This thesis has been written in the supportive academic environment of MetOs. Thank you to all employees at MetOs for showing interest in us master students, giving help and advice, and sharing your enthusiasm for climate science. Thanks to the UiO Cloud group for valuable feedback and discussions, and to the European Research Council for funding MC2. Berit Kaasa at the Institute of Biosciences deserves many thanks for measuring total organic carbon in our sea water samples. I am also grateful to all my fellow students during these last two years for reminding me of why I started on this master's in the first place and generally making life more fun. A very special thanks to everyone in study hall 2418B for being the most life-loving, crazy and caring student family anyone could have asked for. I will truly miss seeing your faces every morning.

Many people have been incredibly important to me during this thesis outside of the university too. I am very grateful for the unconditional support I receive from my mom and dad. Thank you to everyone at Hus for making my home a wonderful place to live, even during a global pandemic, and to the community of Sosialistisk kor. Thanks to all my friends for taking care of me, inspiring me and laughing about life with me, you make me feel very lucky. And to Peder for living everyday life with me.

Finally, thanks to Lånekassen and the Norwegian state for making my education possible. May every student in the world have the same privilege.

Rows and flows of angel hair
And ice cream castles in the air
And feather canyons everywhere
Looked at clouds that way
But now they only block the sun
They rain and snow on everyone
So many things I would have done
But clouds got in my way
I've looked at clouds from both sides now
From up and down and still somehow
It's cloud illusions I recall
I really don't know clouds at all

JONI MITCHELL

Contents

List of Figures

List of Tables

PART I

Introduction and Background

CHAPTER 1

Introduction

1.1 Motivation

The Arctic has warmed almost four times more than the rest of the world in the last 40 years due to anthropogenic climate change (Rantanen et al., 2021). The rapid warming has dramatic consequences for Arctic ecosystems and the livelihood of indigenous peoples. Amongst the global consequences is sea level rise due to glacier and ice sheet melt, and further temperature increase through loss of high albedo surfaces such as snow and sea ice. This pronounced warming in the Arctic compared to the rest of the world is known as Arctic amplification. A number of different climate feedbacks have been proposed to explain it, including the albedo reduction through snow and sea ice loss, confinement of warming to the surface (lapse-rate feedback), increased poleward heat transport in the atmosphere and ocean, and cloud feedbacks (Forster et al., 2021). However, climate models have been shown to underestimate the present Arctic amplification (Rantanen et al., 2021). The uncertainty in the models arise from uncertainty in the multitude of processes affecting Arctic amplification, including cloud feedbacks (Forster et al., 2021).

The role of clouds in Earth's radiative budget is arguably the largest uncertainty in determining the climate sensitivity of the Earth (Forster et al., 2021). Different cloud feedbacks can contribute to both warming and cooling of the Earth, by either trapping more (less) longwave radiation from the surface or reflecting less (more) incoming solar radiation. Part of the uncertainty is due to insufficient knowledge on climate feedbacks of cold clouds (Murray et al., 2021). These can consist of both ice and supercooled liquid water, in which case they are described as mixed-phase. In the mid- to high-latitudes, low-level clouds can contribute to a significant negative climate feedback as increasing temperatures will lead to larger fractions of liquid water in the clouds, which will likely increase the cloud albedo and lifetime (Forster et al., 2021). However, the magnitude of this negative feedback depends on the present supercooled liquid water (SLW) fraction in the clouds (Tan et al., 2016). How this fraction is represented in climate models is very diverging, and leads to substantial differences in model climate sensitivity (Zelinka et al., 2020). Models with a weaker negative cold cloud feedback tend to favour a stronger Arctic amplification (Tan et al., 2019; Forster et al., 2021), making the supercooled liquid fractions of mixed-phase clouds an important area of

research for predicting the development of Arctic and global climate.

In order to represent the SLW fraction correctly in climate models, it is important to correctly represent the concentration of the available ice nucleating particles (INPs). These particles are necessary to initiate heterogeneous ice nucleation, in other words any ice nucleation that occurs above approximately -38 °C (Lamb et al., 2011). The presence of INPs therefore plays an important role in modulating the concentration of ice crystals in cold clouds. However, the concentration of INPs is highly variable in space and time, and there is still insufficient knowledge of the sources and properties of these particles (Kanji et al., 2017). For the Arctic, marine organic aerosol particles from ocean biological activity have been presented as a potentially important source of INPs (DeMott et al., 2016; Wex et al., 2019; Creamean et al., 2019). More knowledge on INP concentrations is particularly important in the high-latitudes, where the low-level cold cloud feedback is especially relevant, but INP concentration measurements are few (Vergara-Temprado et al., 2017; Murray et al., 2021).

1.2 Project description

The objective of this thesis is to investigate the sensitivity of modelled Arctic clouds and radiation to more realistic INP concentrations. We have conducted field measurements of INPs in Andenes on the Norwegian island Andøy, located north of the Arctic circle. To do this we used the newly developed DRoplet Ice Nuclei Counter Oslo (DRINCO) (based on the instrument of David et al., 2019a) to quantify INP concentrations from collected air samples. The measurements were conducted in March of 2021, a period of frequent outbreaks of polar air masses (cold air outbreaks) reaching the measurement site through northerly winds. These observations form the basis of a new parameterisation for Arctic INP concentrations, which is implemented into the climate model NorESM2 (Seland et al., 2020a). Previous modelling studies have included parameterisations for marine organic aerosols to better represent INP concentrations in marine environments such as the Arctic in global climate models. The first was implemented by Yun et al. (2013), and later modelling attempts have shown varying importance of marine organic aerosols for INPs (Huang et al., 2018; Vergara-Temprado et al., 2017; McCluskey et al., 2019). The recent parameterisation of Zhao et al. (2021) shows promising ability to reproduce INP concentrations, but more work is still needed. Ours is a more simplified parameterisation based only on temperature, and is restricted to latitudes above 66.5°N. To our knowledge, this is the first attempt at implementing an observation-based INP parameterisation for the Arctic, dependent only on temperature and latitude. The work in this thesis is centered around the following research questions:

- What are the INP concentrations in Andenes at the time of measurement, how do they compare to other Arctic INP observations and to what extent can they be explained by relevant environmental factors?
- How does the implementation of an observation-based INP parameterisation for the Arctic in NorESM2 affect the ice and liquid content of Arctic

clouds in present day model climate?

- How does the same implementation influence the radiative effect from clouds in modelled present day Arctic climate?

Answering these questions will lay a foundation for discussing the effects and relevance of INPs for future Arctic climate, as well as important directions for future INP modelling work.

1.3 Outline

The rest of the text is organised as follows:

Chapter 2 gives a more detailed theoretical background for the work in this thesis.

Chapter 3 describes the methods used when conducting the observations of Arctic INPs and selected environmental variables.

Chapter 4 includes the methods for climate modelling with and without an observations-based INP parameterisation in the Arctic.

Chapter 5 features the main results of the observational study.

Chapter 6 includes the main effects on modelled climate with and without an observations-based INP parameterisation in the Arctic.

Chapter 7 features a discussion of the representativeness of the observations-based INP parameterisation, its implication for Arctic climate and what this means for future INP modelling.

Chapter 8 gives a summary of the thesis and and an outlook for future work.

Appendix A features additional figures excluded from the main results.

Appendix B lists how the data and computer code used in this thesis can be accessed.

CHAPTER 2

Background

This chapter presents the theoretical background central to this thesis. A general description of what ice nucleating particles (INPs) are and what characterises them are given in Section 2.1. The role that these INPs play for cloud phase is described in Section 2.2. In Section 2.3, the influence of cloud phase on climate and some of its associated climate feedbacks are presented. Lastly, there is a short introduction in Section 2.4 to earth system modelling and the challenges of modelling processes on a scale far below the model resolution.

2.1 Characterisation of INPs

The formation of ice in the atmosphere requires water molecules to bind together in a crystalline structure. This happens through stochastic molecular movement, through which clusters of water molecules can form ice phase structures, but the probability of a cluster decaying instead of growing is higher until the cluster reaches a critical size. The likelihood of the cluster reaching this size is dependent on temperature and relative humidity, and this is the phenomenon we know as ice nucleation (Vali et al., 2015). At temperatures above -38°C, the energy barrier associated with ice nucleation is too high for water molecules to form ice spontaneously, but the barrier that needs to be overcome can be lowered by the presence of an INP (Kanji et al., 2017). The surface of a foreign substance, the INP, can provide a site that aids the water molecules in forming a crystalline structure, and thereby initiate ice nucleation at temperatures between -38°C and 0°C. This is known as heterogeneous ice nucleation, as opposed to homogeneous ice nucleation, which occurs without the influence of foreign substances, at temperatures below -38°C.

Heterogeneous ice nucleation can occur in different modes. The terminology used to describe these modes here is from Vali et al. (2015), but it should be mentioned that this terminology has differed in the past, and may change in the future. *Deposition nucleation* denotes ice nucleation where supersaturated vapor deposits directly onto an INP without any prior presence of liquid water. For porous particles it is unclear whether ice nucleation that occurs below water saturation or in the deposition nucleation mode is actually so-called pore condensation and freezing, where water condenses in pores or cavities below water saturation due to capillary effects, as suggested by Marcolli (2014) and shown by e.g. David et al. (2019b). *Immersion freezing* is

the process of ice nucleation that occurs due to an INP immersed in a liquid droplet. Once the INP-containing droplet reaches a certain supercooling, the immersed INP will initiate the freezing of the droplet. *Condensation freezing* refers to the process of liquid condensing onto an INP at temperatures below 0°C, followed by freezing. However, there is little evidence that condensation freezing is truly different from immersion freezing or deposition nucleation at a microscopic scale (Vali et al., 2015). *Contact freezing* describes the initiation of ice nucleation due to an INP coming into contact with a liquid water droplet, with ice forming at the air-water or air-liquid-particle interface.

As of today, there is no conclusive evidence of what makes an aerosol particle an INP. Traditionally, INPs have been characterised as insoluble and with a structure that resembles the ice lattice, or with other physical properties that make up ice formation-favorable sites known as ice-active sites (Kanji et al., 2017). The larger the particle, the higher the probability that it contains an ice-active site, and particles of diameter < 0.5 μm have been thought to be less likely to act as INPs (DeMott et al., 2010). However, this idea has been challenged by more recent studies. Nanoscale biological fragments, such as pollen macromolecules, fungal spores and marine organic aerosols, have been shown to act as ice nucleators (Pummer et al., 2012; Fröhlich-Nowoisky et al., 2015; Wilson et al., 2015). This shows that there is not necessarily a lower size threshold for INPs. The insolubility requirement has also been challenged by studies of deliquesced salt (Niehaus et al., 2015) and effloresced ammonium sulfate particles (Abbatt et al., 2006). As such, further clarification is needed in defining what physical properties give an aerosol particle a high ice nucleating ability.

However, there are many known sources of INPs. These include, amongst others, mineral and desert dust, pollen, spores and plant fragments from vegetation, biologically enriched sea spray from the ocean, ash from volcanoes and biomass burning, and anthropogenic emissions such as agricultural dust and soot from fossil fuel combustion (Kanji et al., 2017). There is strong regional and seasonal variability in the strength of many of these sources. Even though the abundance of primary biological aerosols is generally less than that of mineral dust (Després, 2012), they become more important as sources of INPs in areas where dust is absent. Wilson et al. (2015) found that in areas such as the Southern Ocean, the North Atlantic and the North Pacific, INP concentrations at -20°C at 850 hPa largely originate from marine organic aerosols, and that dust was of less importance. In the high latitudes, such as the Arctic and the area of focus in this thesis, the air is relatively pristine compared to lower latitudes, and the ocean is therefore thought to be an important source of INPs in this area (Burrows et al., 2013; Vergara-Temprado et al., 2017; Irish et al., 2017). Bubbles can scavenge biological material in the ocean while rising, leading to a thin organically enriched layer at the surface known as the sea surface microlayer (Wilson et al., 2015). This material, when ejected into the atmosphere through bubble bursting and sea spray, forms marine organic aerosols that can act as INPs (DeMott et al., 2016).

2.2 The role of INPs for cloud phase

Even though INPs can play a role in cirrus cloud formation, where temperatures are usually below the homogeneous freezing temperature, the role of INPs is potentially more significant in mixed-phase clouds, where INPs are the only source of primary ice production. In these cloud types, immersion freezing is believed to be the most dominant process of heterogeneous ice nucleation, supported by observational studies indicating that liquid water droplets are a prerequisite for ice formation in mixed-phase clouds (Ansmann et al., 2008; Boer et al., 2011; Westbrook et al., 2013). However, ice can also be produced in mixed-phase clouds without the presence of INPs as long as some ice is already present, e.g. through ice falling from above. This is known as secondary ice production (SIP). Mechanisms of SIP include splintering of rimed crystals, fragmentation by crystal collisions, splintering produced when large droplets freeze (droplet shattering) and fragmentation of crystals through sublimation (Field et al., 2017; Korolev et al., 2020). The presence of SIP can explain the discrepancy often observed between ice crystal number concentrations and ambient number concentrations of INPs (Auer et al., 1969; Mossop, 1970). This discrepancy has a tendency to increase with increasing temperatures, indicating that SIP is most effective at higher temperatures. Indeed, the rime splintering mechanism, often referred to as the Hallett-Mossop process, is most effective at around -5°C (Hallett et al., 1974). This further complicates the "ice production potential" of known INP types. While INPs from mineral dust are more abundant than biological INPs, their freezing temperatures are usually less than -20°C (Murray et al., 2012), while biological INPs freeze at higher temperatures (Hoose et al., 2012). Since these higher temperatures might be more favorable for SIP, biological INPs could still contribute to high ice number concentrations even though the primary biological aerosol concentrations are generally lower. To summarize, although INPs are essential for primary ice formation, their concentrations alone do not determine the cloud phase partitioning of mixed-phase clouds. SIP also plays an important role, but there is an incomplete understanding of the complex physical mechanisms behind it (Field et al., 2017).

2.3 The influence of cloud phase on climate

Cloud phase matters for climate in many respects. It influences cloud radiative properties, cloud lifetime and precipitation. Cloud glaciation, or the rapid growth of ice crystals within a mixed-phase cloud, leads to fewer and larger particles that precipitate more easily. This results in optically thinner clouds, which reflect or absorb less radiation, as well as shorter-lived clouds due to the earlier onset or increased possibility of precipitation. Rapid growth of ice crystals within a cloud at the expense of liquid cloud droplets is known as the Wegener–Bergeron–Findeisen (WBF) process (Wegener, 1911; Bergeron, 1935; Findeisen, 1938), and is a result of the lower saturation vapor pressure over ice compared to that over water. This means that if the ambient vapor pressure falls between the saturation vapor pressure over water and the saturation vapor pressure over ice, ice particles can grow rapidly at the expense of liquid water if ice is present. The WBF process has been shown to have large implications for the climate impacts of mixed-phase clouds (Storelvmo et al., 2015).

On the other hand, a higher supercooled liquid water content in clouds entails a higher number of smaller droplets which increase the cloud surface area and the optical thickness. The degree to which the optical thickness influences cloud radiative properties is different for shortwave and longwave radiation. While cloud albedo, or the shortwave reflective properties of clouds, increases quite linearly with increasing optical thickness (Twomey, 1974), the longwave absorptivity and emissivity of clouds increases non-linearly with cloud liquid water content (Stephens, 1978). This happens in such a way that a relatively small increase in cloud liquid water content can lead to a large increase in the downwelling longwave radiation from clouds if the water content was low to begin with. However, if the longwave emissitivity of the clouds is already close to 1, the increase of water content will have little effect on increasing the longwave cloud radiative effect.

In general, cloud climate effects make up a large source of uncertainty in global climate predictions. The overall feedback from clouds in a warming climate is assessed to be positive by the latest report from the Intergovernmental Panel on Climate Change (IPCC; Forster et al., 2021), but the feedback effects in different cloud regimes are diverging. The role of cloud phase is generally thought to be a negative feedback, as increasing temperatures will increase the liquid content of mixed-phase clouds, thereby increasing the cloud albedo and reflecting more sunlight back to space. This feedback is of special relevance in the southern extratropics, where mixed-phase clouds over the Southern Ocean account for 20 % of the global cloud radiative effect in the present climate (Forster et al., 2021). The feedback is state-dependent, since it only has an effect as long as temperatures are below freezing temperatures (Bjordal et al., 2020), and is also largely dependent on the amount of ice in present day clouds. Underestimation of the supercooled liquid fractions of Southern Ocean clouds has previously led to an overestimation of the negative ice cloud feedback, and the feedback has been shown to reduce in magnitude when supercooled liquid fractions are constrained by present day observations (Tan et al., 2016). The overall increased climate sensitivity in phase 6 of the Coupled Model Intercomparison Project (CMIP6) has been shown to be strongly correlated with the strength of the extratopical low cloud climate feedback in the climate models (Zelinka et al., 2020), in which the negative cloud phase feedback plays an important role. These findings underline the need for realistic representation of ice formation in mixed-phase clouds in order to correctly estimate climate sensitivity.

The Arctic cloud regime, the focus of this study, is characterised by low clouds forming in a stable boundary layer. The Arctic sea ice plays a large role in mediating moisture fluxes to the atmosphere, and the declining sea ice in a warmer climate is therefore thought to enhance cloud formation, especially in summer and early fall (Forster et al., 2021). Due to the seasonal differences in incoming solar radiation, the climate effects of Arctic clouds have a strong seasonal dependence. Cloudier conditions during boreal autumn and winter due to sea ice loss have been estimated to result in more downwelling longwave radiation and heating of the surface (Kay et al., 2009), indicating that Arctic clouds have positive feedback at the surface. The Arctic cloud feedback at the

top of the atmosphere is also estimated by the IPCC to be slightly positive, but with low confidence (Forster et al., 2021). As there is less vertical coupling in the atmosphere over the Arctic, however, it is most relevant to consider the radiation budget at the surface to understand climate effects in this region (Pithan et al., 2014). Based on the unknowns mentioned above, investigating the climate effect of cloud phase changes in the Arctic in the present climate, using the second generation of the Norwegian Earth System Model, is a central area of research in this thesis.

2.4 Earth system modelling of cloud ice microphysics

An Earth System Model (ESM) is a discretized mathematical representation of the Earth. It models the different spheres of the globe (the atmosphere, hydrosphere, cryosphere, biosphere and lithosphere) through the primitive equations of movement and conservation, as well as various parameterisations (Lenton, 2016). An ESM couples the spheres together and allows them to interact with each other. The numerical resolution of an ESM is finite in space and time, and as with model complexity it is limited by computational capacity. Parameterisations are in place to represent processes happening at scales below the model resolution, of which cloud microphysics is a clear example. Uncertainty in these parameterisations is a major source of overall model uncertainty (Otto, 2012), as the parameterisations necessary for ESMs are usually significant simplifications of the actual processes they represent. This thesis, however, consists partly of an ESM study. ESMs are usually distinguished from general circulation models (GCMS) by having interactive carbon cycling (Lenton, 2016), and for all practical purposes the modelling study in this thesis is no different from a GCM study. The challenges, however, remain the same.

While ESMs are not able to capture cloud dynamics as well as cloud resolving models (CRMs) of a finer resolution, they are a necessary tool for estimating the large-scale climate effects of cloud microphysics, such as the effect on Earth's radiation budget. However, the coarse resolution of ESMs can exclude many important mechanisms for cloud ice microphysics. To mention a few, the models do not resolve vertical velocities at cloud scale, and do not capture sub-grid box temperature fluctuations that could matter for ice formation (Kanji et al., 2017). The signal from changing the parameterisation of an ice formation mechanism can be averaged out by the coarse resolution or overshadowed by model dynamics, requiring careful interpretation of the modelling results.

Neither CRMs or ESMs are able to capture physical processes at the microlevel, and improvement of ice nucleation representation in both model types includes the challenging task of creating simplified parameterisations that are simultaneously physically based. In this thesis, the impact of implementing an INP parameterisation limited to the Arctic is studied. This violates one of the common sense rules for climate model parameterisations presented by Otto (2012), namely that parameters should relate to physical processes and not to specific geographic areas. As this thesis is not at attempt to improve

the ESM parameterisation, but a study of the sensitivity of the ESM to an observation-based parameterisation adjustment, this rule violation is of lesser relevance. However, in the future INP parameterisations in ESMs should be based on known physical relationship and processes relating INP concentrations and ambient factors (such as ocean biology, vegetation, etc.), in order to fully quantify the effect of these particles in a changing climate. For this to be possible, a greater understanding of INPs and cloud microphysics is necessary. To transform improved process understanding into improved ESMs is then a path paved with trade-offs. While using computational capacity to increase model resolution can lead to improved representation of cloud processes, creating more complex parameterisations for predicting INP concentrations also demands greater computational power (Kanji et al., 2017). None of these model improvements are necessarily in conflict with each other, and future modelling solutions could allow smarter spending of computational power. The more relevant subject is perhaps that it is impossible to include all the processes determining INP concentrations in a single parameterisation, and that choices need to be made regarding which processes to include, and which to exclude. What direction the models should go in will depend on what questions the models should answer.

PART II

Methods

CHAPTER 3

Observational methods

A description of the observations conducted in this thesis, primarily the ice nucleating ability of air and sea water samples, is given in Section 3.1. In Section 3.2, a description of the instruments used to conduct the measurements is given. The methods for postprocessing of the observational data can be found in Section 3.3. Finally, there is a description in Section 3.4 of how the air sample measurements were used to create a parameterisation of INP concentrations per litre as a function of temperature. This parameterisation is used in the modelling methods in Chapter 5. The scripts for data postprocessing, analysis and visualisation can be found in Appendix B.

3.1 Data collection

The collection of observational data was conducted at Andenes in Andøy Municipality in Norway, located at 69°18'N, 16°07'E. The location of the data collection site is shown in Figure 3.1.

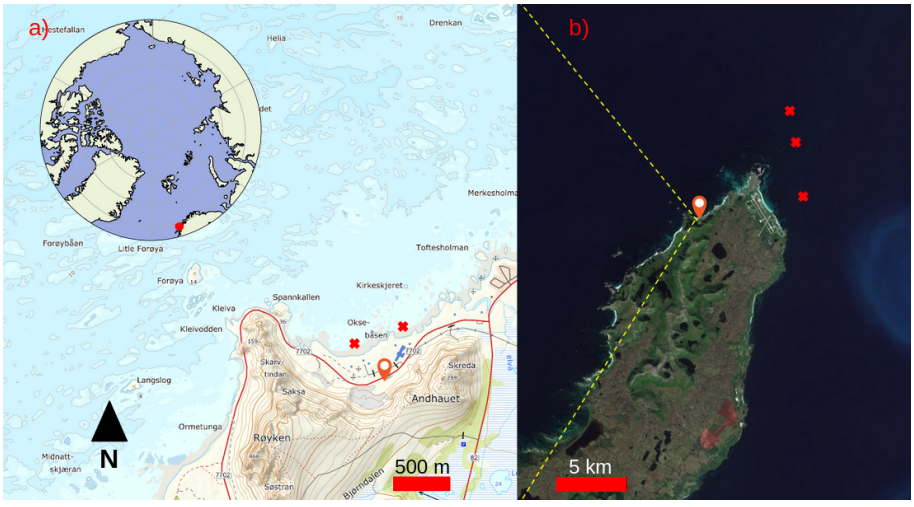

Figure 3.1: Map of data collection site at Andenes, Norway (*Kartverket* 2022). The air sampling site (red pin) and shore water collection sites (red crosses), as well as Andøy's position in the Arctic, can be found in panel a). Other seawater collection sites (red crosses) can be found in the aircraft picture in panel b).

The aerosol collection site (marked with red pin in Figure 3.1a) is situated at sea level around two hundred meters from the North-facing shore, and is shielded from the south by mountains that rise approximately 200-400 meters above sea level. The air was sampled through an inlet located approximately 6 meters above ground, using the Coriolis liquid impinger described in Section 3.2. The temperature of the air inlet, as well as the aerosol concentration, was measured continuously. The air samples were collected during the period 2021-03-15−2021-03-30, and were analysed immediately or stored at -18°C and analysed within a few days, following Beall et al. (2020).

The collection site for sea water samples is at the North-facing shore. The samples were collected from two adjacent bays (marked with red crosses on Figure 3.1a), a few meters into the water where turbulence from wave-breaking at the shore was less prevalent. In order to investigate the ice nucleating properties of the ocean surface layer with potential to be emitted into the air, only the top layer of the water was sampled. Temperature of the sea water was also measured, and the total organic carbon (TOC) content of the samples was analysed. Three surface layer sea water samples were also collected from boat on the open sea at the east side of Andøy (marked with red crosses on Figure 3.1b) by Eve Jourdain at the University of Oslo (Institute of Biosciences; Department of Aquatic Biology and Toxicology). All samples were collected during the period 2021-03-18−2021-03-30, and while some were analysed immediately after sampling, some were also analysed up to five months after sampling. They were stored at -18°C temperatures, but due to the long storage time it should be noted that they might be prone to ice nucleating ability degradation (Beall et al., 2020).

Pressure and wind data in Andøy Municipality from the sampling period was accessed through the Frost API, which provides free access to MET Norway's archive of historical weather and climate data.

The observational data in this thesis was collected as a part of the 2021 field campaign of the research projects MC2 and ISLAS, and is the work of multiple researchers in MC2. The field campaign was based in the research facilities of Andøya Space.

3.2 Instrument description

The Coriolis setup

For the collection of aerosols, a Coriolis-μ high flow liquid impinger (Bertin Instruments, France) was used. The intake of the Coriolis was connected to the inlet tube, as can be seen in Figure 3.2. A cone-shaped collection flask to sample the aerosols was filled with 15 ml of purified water (W4502, Sigma-Aldrich, USA) before sampling. During aerosol sampling, the Coriolis sampled air through the inlet at a flow rate of 300 L/min for 40 minutes. As the air is sampled, it rotates inside the cone-shaped flask, causing particles (mainly larger than 400 nm) to be scavenged by the purified water due to their inertia. The flow of the air is illustrated with the cyan line in Figure 3.2. As some of the water evaporates, more purified water is pumped into the flask at a fixed pump rate during sampling. At the end of the sampling period, the resulting water

volume of the cone is measured, and the ice nucleating ability of the particles immersed in the water is ready to be further analysed. While not sampling, the tube between the Coriolis intake and the air inlet is closed by a 3-way valve (Model 120VKD025-L, Pfeiffer Vacuum, Germany), and the flow of the inlet is instead maintained by a blower (Model U71HL, Micronel AG, Switzerland), as indicated by the red line in Figure 3.2.

Optical Particle Counter

The aerosol concentrations were measured with an Optical Particle Counter (OPC; Met One GT-526S). The OPC measures the number of particles per litre of air exceeding certain sizes in bins, i.e. the number of particles with diameter greater than 0.3 μm, 0.5 μm, 0.7 μm, 1 μm, 2 μm and 3 μm. As the OPC does not count particles smaller than 0.3 μm, it excludes potential nanoscale biological aerosols, described in Section 2.1. We therefore mainly consider particles with a diameter above 0.5 μm when we compare aerosol concentrations to INP concentrations, which is the size that has traditionally been considered most relevant for INPs (DeMott et al., 2010; Kanji et al., 2017).

Temperature Logger

The inlet and sea water temperatures were recorded using a Thermocouple Data Logger (EL-GFX-TC, Lascar Electronics).

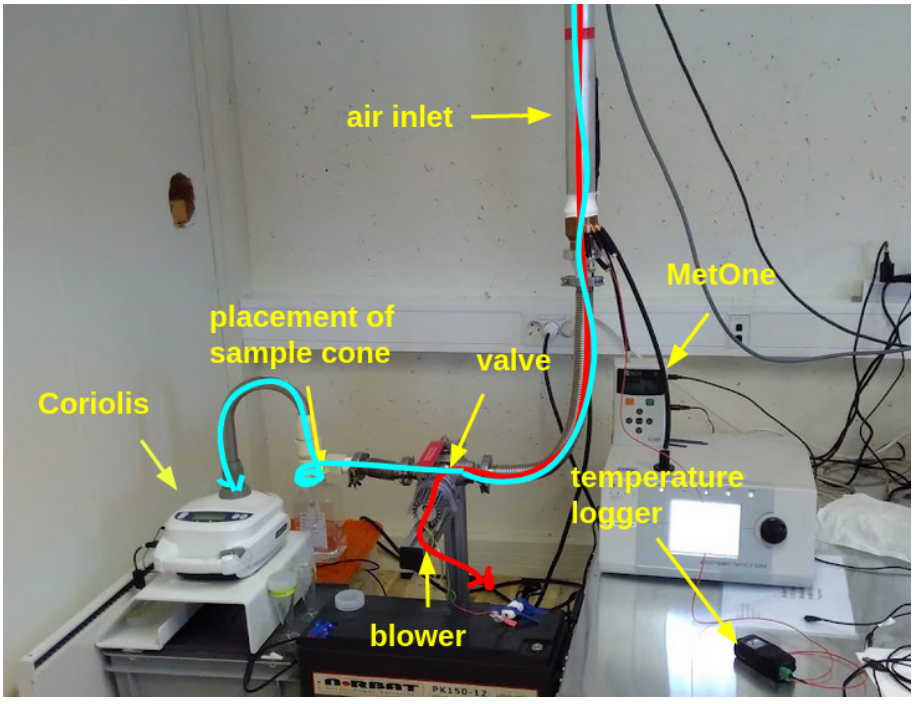

Figure 3.2: The air sampling setup, including a cyan line to indicate the direction of air flow while sampling, and a red line to indicate the direction of the air flow while not sampling.

DRINCO

The ice nucleating ability of the air and water samples was determined using the DRoplet Ice Nuclei Counter Oslo (DRINCO). DRINCO is based on the DRoplet Ice Nuclei Counter Zürich, developed by David et al. (2019a) and with some updates described by Miller et al. (2021). The instrument has been validated using purified water with different mass concentrations of NX-illite (not shown), which has a well documented freezing temperature (David et al., 2019a). An image of the instrument and its principle components is shown in Figure 3.3a.

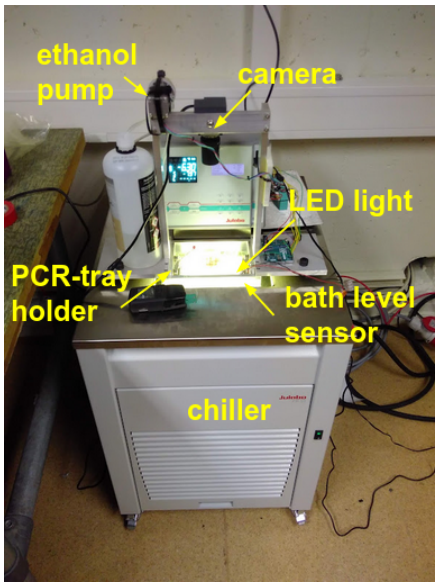

(a) The DRoplet Ice Nuclei Counter Oslo (DRINCO) setup, consisting of a cooler with ethanol, a pump regulating the ethanol level, a PCR tray which is lowered into the ethanol bath and a camera above the tray.

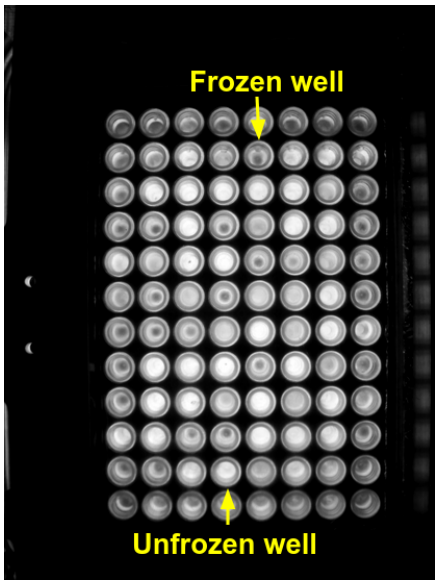

(b) A sample distributed in a PCR tray, midway through freezing, as observed by the instrument camera. The darker circles are frozen wells, while the brighter circles are still unfrozen.

Figure 3.3: Description of the DRINCO instrument.

The instrument consists of an ethanol bath, which is temperature-controlled by a chiller (FP51, Julabo), into which a custom-designed tray-holder for PCR-trays can be placed. The PCR-tray (732-2386, VWR, USA) consists of 96 wells, where 50 μl aliquots of a liquid sample are pipetted into. The instrument is equipped with a bath leveler consisting of a bath level sensor (LLC102000, SST, UK) and a peristaltic pump (KAS-S10, Kamoer, China), to ensure that the level of the ethanol bath always aligns with the sample level in the wells. This is to prevent the well walls adjacent to the air above the water from cooling faster than the rest of well, and thus prevent condensation on the well walls that could potentially slide back into the aliquots and lead to premature freezing through percussion freezing (Marcolli, 2017). A waterproof LED light is placed beneath the tray holder to transmit light through the wells, which is captured by a camera (ELP-USB8MP02G-SFV, SVPRO, China) above the sample tray. The

sample is cooled at a fixed rate of approximately -1°C/min from -2°C to -32°C, or as long as it takes for all the wells in the tray to freeze. The camera takes a picture every 15 seconds, corresponding to a picture every 0.25°C. When a well freezes, the light transmitted through the wells decreases, as can be seen in Figure 3.3b. The pictures are analysed with a `MATLAB` code, which registers the position of each well and the change in their light intensity during the experiment. The bath temperature that corresponds with the largest drop in light intensity for each well is registered as the well freezing temperature. The measurement results in a frozen fraction of the sample at each temperature.

TOC analyser

For measurements of total organic carbon (TOC), a TOC-V (TOC 5050A, Shimadzu) analyser was used. The measurements were conducted by Berit Kaasa, senior engineer at the University of Oslo (Institute of Biosciences; Department of Aquatic Biology and Toxicology). The Shimadzu works by delivering the sample to a combustion furnace, which is supplied with purified air. There, it undergoes combustion through heating to 680°C with a platinum catalyst. It decomposes and is converted to carbon dioxide gas. The carbon dioxide is cooled and dehumidified, and then sent to a detector where the concentration of total carbon in the sample is obtained by a comparison with a standard calibration curve formula.

3.3 Data postprocessing

Temperature calibration of DRINCO

The ethanol in the chiller bath is not cooled uniformly, but circulates in order to remain well-mixed. Therefore, there is a slight temperature difference across the tray. There is also a time lag between the bath temperature communicated by the chiller to DRINCO and the actual temperature measured at different parts of the tray. In order to account for some of these temperature differences, a temperature calibration was conducted. This was done by filling the tray wells with 50 uL of ethanol (95 %, Antibac), and measuring the temperature of the four corners and a center well, while cooling the tray. Afterwards, the temperature registered by DRINCO was compared to the actual temperatures measured across the tray. This is the same calibration procedure as used by David et al. (2019a). The result of the temperature calibration can be seen in Figure 3.4. The temperature calibration was then constructed using a linear fit between the lines using the `LinearRegression` function of the `Python` package `sklearn`. When doing so, we obtain an average corrected temperature across the tray of $0.30 + 0.89 \times T_{DRINCO}$, where T_{DRINCO} is the temperature registered by DRINCO. This average temperature correction is applied to the ice nucleation measurements.

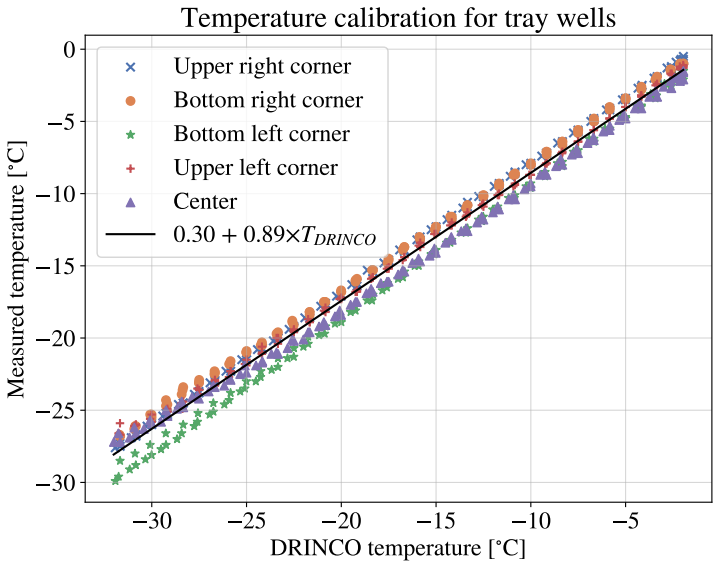

Figure 3.4: Measured temperatures for the four corner wells of the tray, as well as the center well, compared to the temperature of the chiller as registered by DRINCO.

Conversion to INP concentration per standard litre of air

Following Vali, 1971, the cumulative concentration of INPs in a sample at a given temperature, $K(T)$ can be calculated as

$$K(T) = \frac{-\ln(1 - FF(T))}{V_{droplet}}, \tag{3.1}$$

where $FF(T)$ is the fraction of sample droplets which are frozen at the given temperature, and $V_{droplet}$ is the volume of the droplets. In our case, this volume corresponds to the liquid content in the tray wells. This calculation assumes that all drops have the same chance to contain INPs. There is also a probability that there are more than one INP present in each drop that can lead to freezing at each given temperature. However, due to the rarity of these events when using temperature intervals and volumes as small as ours, this possibility is neglected in our calculations. The probability of more than one INP initiating freezing at a given temperature in one droplet can be calculated using Poisson's law (Vali, 1971).

When converting the frozen fraction of our air samples to a cumulative concentration of INPs in a unit volume of air, $K_{air}(T)$, we also need to consider how much air we have sampled, as well as what amount of water the air particles have been sampled in. This is done by dividing the cumulative concentration $K(T)$ by the volume of air V_{air} over the sample volume V_{sample}, resulting in the equation

$$K_{air}(T) = \frac{-\ln(1 - FF(T))V_{sample}}{V_{droplet}V_{air}}. \tag{3.2}$$

As the sampled air mass in a volume may vary due to temperature and pressure variations, we convert the volume unit in our concentration from actual litre to standard litre, using the ideal gas law, a reference temperature $T_{std} = 273.15$ K and a reference pressure of $p_{std} = 1013.5$ hPa. The ideal gas law on the form $V = Nk_BT/p$ was used to perform the conversion, where V is volume, N is number concentration, T is temperature, p pressure, and k_B is the Boltzmann constant. The conversion from number concentration N per sampled volume V to N per standard volume V_{std} was performed in the following way:

$$\frac{N}{V_{std}} = \frac{N}{V} \times \frac{V}{V_{std}} = \frac{N}{V} \times \frac{Nk_BT/p}{Nk_BT_{std}/p_{std}} = \frac{N}{V} \times \frac{p_{std}}{p} \times \frac{T}{T_{std}}. \tag{3.3}$$

The INP concentration at a given temperature per standard litre of air, $K_{std}(T)$, is then calculated as

$$K_{std}(T) = K_{air}(T) \times \frac{p_{std}}{p} \times \frac{T}{T_{std}}, \tag{3.4}$$

where p is the ambient air pressure and T is the measured inlet temperature in Kelvin. Equation 3.4 was also used to calculate aerosol concentrations per standard litre.

Calculation of total aerosol surface area

The surface area of the total number of aerosol particles measured by the OPC was calculated under assumption that the particles are spherical, following DeMott et al. (2016). The surface area A of each particle was calculated as $A = 4\pi(d/2)^2$, where d is the diameter of the particles. This assumption likely does not hold for all particles, and could be a potential source of error.

Conversion to cumulative INPs per gram TOC in sea water

To be able to compare our study to the study of Wilson et al. (2015), we calculated the cumulative number of INPs per gram of TOC in the collected sea water samples. This was done by first finding the cumulative INP number per litre of sea water, following Equation 3.1, and subsequently dividing this number by the grams of TOC present per litre of sea water found for each sample.

Linear interpolation of TOC

As we are interested in comparing the TOC concentration in sea water with the freezing temperatures of INPs sampled by the Coriolis, but the TOC measurements only have a daily resolution, they have been linearly interpolated between measurements. This interpolation was performed using the `interpolate` function from the `Python` library `pandas`.

Freezing point depression of sea water

When analysing the freezing temperatures of INPs in sea water, we account for the depressed freezing point due to the salt content of the water by applying a temperature correction of $+1.8$°C to all measurements. As we have not

been able to measure the actual salinity of each sample, we use this value for the temperature correction since -1.8°C is known as a typical freezing point depression for Arctic waters (Wadhams, 2000). However, it should be noted that this method entails some uncertainty.

3.4 Parameterisation of INP concentrations

Based on the measurements of INP concentrations in the air at Andenes in 2021, we created a parameterisation of INP concentrations as a function of temperature. In order to do this, an exponential fit is performed by first making a linear regression of the the logarithm of the INP concentration per standard litre of air, using the `polyfit` function from the `Python` package `NumPy`, and then taking the exponential of the linear regression. This procedure is performed both for all the measurements and the measurements excluding a high value outlier, taken at a time of high southerly wind speeds when sea spray was visible and likely entering the inlet during sampling. The parameterisations can be seen in Figure 5.1.

CHAPTER 4

Modelling methods

To investigate the sensitivity of Arctic clouds and radiation to changes in Arctic ice nucleating particle (INP) concentrations in an Earth System Model, the parametrisation for INPs is updated to be representative for Arctic INP concentrations based on observations from Andenes in 2021. For this purpose the second generation of the Norwegian Earth System Model (NorESM2; Seland et al., 2020a) was used. A general description of NorESM2 is provided in Section 4.1, and a description of the heterogeneous ice nucleation mechanisms in the atmospheric component in Section 4.2. After that, a detailed description of the model experiments is given in Section 4.3. Moreover, the postprocessing of the model data (Section 4.4) and the spatial and temporal averaging of the data (Section 4.5) are presented. Finally, a description of the model cloud phase metrics used for the direct comparison with LiDAR data and the details of this data, is given in Section 4.6. Information about the model version, model modifications and data processing scripts can be found in Appendix B.

4.1 Description of NorESM2

The Norwegian Earth System Model (NorESM) (Bentsen et al., 2013; Iversen et al., 2013; Kirkevåg et al., 2013; Kirkevåg et al., 2018; Seland et al., 2020a) is a branch of the Community Earth System Model (CESM) (Hurrell et al., 2013; Danabasoglu et al., 2020), and NorESM2 is based on the second generation of CESM (CESM2). The two models share code infrastructure and many of the same characteristics. NorESM2 differs substantially from CESM2 in using a completely different ocean component, the Bergen Layered Ocean Model (BLOM; Bentsen, 2020), as well as a different ocean biogeochemistry component, the Hamburg Ocean Carcon Cycle (iHAMOCC) model (Tjiputra et al., 2020). In addition, the atmosphere component of NorESM2 (CAM6-Nor) differs from the Community Atmosphere Model of CESM2 (CAM6) in its use of a different atmospheric aerosol module (OsloAero6: Kirkevåg et al., 2018). The CAM6-Nor also differs from CAM6 in its improved conservation of energy and momentum, as well as its parameterisation of turbulent air-sea fluxes (Toniazzo et al., 2020). The sea-ice model component, based upon version 5.1.2 of the sea-ice model CICE (Hunke et al., 2015), and the land model component based upon version 5 of the Community Land Model (CLM5; Lawrence et al., 2019), have minor modifications (Seland et al., 2020a). Both CESM2 and NorESM2 have been used to contribute to the sixth and latest generation of the Coupled Model

Intercomparison Project CMIP6 (Eyring et al., 2016). As the goal of this modelling study is to investigate the sensitivity of clouds and radiation to INPs, only the atmospheric component of NorESM2 is used. The atmosphere component we use has a $2.5° \times 1.875°$ ($\sim 2°$) horizontal resolution, 32 hybrid-pressure layers in the vertical and a "rigid" lid at 3.6 hPa (40 km) (Seland et al., 2020a).

4.2 Heterogeneous ice nucleation in CAM6 and CAM5

Most central to the modelling study in this thesis is how NorESM2 represents ice nucleation at mixed-phase cloud temperatures and the effect of this representation on the model climatology. Though CAM6-Nor, the atmospheric component of NorESM2, has a different aerosol module than its parent component CAM6 in CESM2, the microphysics related to heterogeneous ice nucleation is the same for both CAM6-Nor and CAM6. "CAM6-Nor" and "CAM6" are therefore used interchangeably when describing the heterogeneous ice nucleation in the model.

CAM6 uses a heterogeneous ice nucleation scheme based on classical nucleation theory, following Hoose et al. (2010). This scheme has replaced three individual parameterisations in the previous component version CAM5, representing different paths to heterogeneous freezing. The first path is contact freezing, which follows Young (1974). The second path is immersion freezing, which follows Bigg (1953) (hereafter: B53). The final path is deposition and condensation freezing, which follows Meyers et al. (1992) (hereafter: M92). The classical nucleation theory (CNT) scheme in CAM6 has a well-documented bug, consisting of an ice number concentration limit that has been shown to prevent heterogeneous nucleation processes from nucleating ice crystals (Shaw et al., 2022), making it unsuitable for studying sensitivity to INP concentration adjustments. In addition, it calculates the atmospheric ice nucleation based on temperature and the surface area of dust aerosols in each time step. As we expect that marine organic aerosols might be equally or more important than dust for Arctic (Vergara-Temprado et al., 2017; Wex et al., 2019), a purely dust-based INP scheme is either way less suited for our purposes. Our measurements of INPs in the Arctic do not show a clear relationship between aerosol surface area and ice nucleating ability. Instead, temperature is the most important factor determining INP concentrations, similar to Li et al. (2022). It therefore makes sense to return to the parameterisations of CAM5, instead of using the CAM6 scheme, when adjusting the Arctic INP concentrations in the model to our measurements at Andenes in 2021. We have chosen to apply this change to M92, which is active in the mixed-phase cloud regime at temperatures between -37°C and 0°C. While B53 is of immersion freezing, and M92 is not, B53 is dependent on the size distribution of the droplets (Bigg, 1953). However, the size of the droplet in which an ice nuclei is immersed should not matter for the temperature at which an INP is activated. M92 is dependent only on the saturation vapour pressures over ice and water, which are temperature-dependent functions, and is therefore the most relevant to change for this thesis. Since we have measured INPs in the immersion mode, replacing the M92 with our measurements entails excluding deposition and

condensation freezing mode nuclei for mixed-phase clouds in the Arctic. This exclusion is justified by observational studies indicating that deposition and condensation freezing is of little importance for mixed-phase clouds (Ansmann et al., 2008; Boer et al., 2011; Westbrook et al., 2013), as described in section 2.2.

4.3 Model experiments

A full list of performed model experiments conducted in this thesis are presented in Table 4.1. The details of the experiments are described further down in this section. The setup is the same for all experiments apart from the differences apparent from the experiment descriptions in the table. The model setup shared by the experiments is listed in Table 4.2.

Name	Description
CAM6	Heterogeneous ice nucleation as in CAM6 without ice number limit
CAM5	Heterogeneous ice nucleation as in CAM5 and no further changes
Andenes 2021	Heterogeneous ice nucleation as in CAM5 with changes to parameterisation of Meyers et al. (1992) in the Arctic based on Andenes 2021 INP measurements

Table 4.1: List of NorESM2 model experiments

Shared experiment setup

The model run setup of the experiments, or the "compset", is called "NF2000climo", and defines only the atmosphere to be active (Seland et al., 2020b). The other components of the model are represented using input files that act as boundary conditions to the atmosphere. These input files are defined by present day climate. While the temperatures over land and sea ice can respond to energy fluxes from the atmosphere, it is important to note that the sea surface temperatures do not. Further, the atmospheric circulation is nudged by ERA-Interim reanalysis data of pressure and wind fields (Dee et al., 2011). This nudging still allows the atmospheric model to respond to forcing changes due to changes in heterogeneous ice nucleation. However, the signal from the differences in ice nucleation between experiments emerges more quickly with a nudged circulation, as the random difference in climate variability between experiments is suppressed (Dee et al., 2011). This allows a relatively short simulation length while still seeing a clear signal, which is also the reason why we have chosen to not include significance estimates of the changes between model runs. The length of the model runs is three years, with an additional three months added to allow for the model to spin up.

Individual experiment descriptions

Below follows short, individual descriptions of the performed model experiments. Note that the sourcecode modifications and given namelist options for each

Specification type	Specification	Explanation
Compset	NF2000climo	A predefined NorESM2 model run setup with prescribed sea surface temperatures and present day climate
Resolution	f19_tn14	$\sim 2°$ resolution
Run type	Startup	Initialisation using default files
Start date	2007-01-01	
Simulation length	39 months	
Nudge files	ERA_f19_tn14	2° resolution ERA-Interim reanalysis data for pressure and wind fields

Table 4.2: Overview of shared setup for NorESM2 model experiments

experiment can be found in Appendix B.

CAM6

"CAM6" is used to refer to the model experiment using the heterogeneous ice nucleation physics in CAM6, as described in Section 4.2. The only change made to the model setup is to remove the limitation on ice number concentration that has been shown to prevent heterogeneous nucleation processes from nucleating ice crystals (Shaw et al., 2022). The purpose of this experiment is to have a NorESM2 baseline to compare against when changing the heterogeneous ice nucleation physics in the model back to how it was in CAM5.

CAM5

"CAM5" is used to refer to the model experiment using the default heterogeneous ice nucleation physics in CAM5, as described in Section 4.2. The purpose of this experiment is to have a baseline to compare our adjustment to heterogeneous ice nucleation in the Arctic against.

Andenes 2021

"Andenes 2021" is used to refer to the model experiment using the heterogeneous ice nucleation physics in CAM5, with an adjustment to heterogeneous ice nucleation in the Arctic based on measurements in Andenes 2021. In this experiment the activated ice number produced by the parameterisation of Meyers et al. (1992) is replaced in the atmospheric column if the latitude of the column exceeds 66.5°N. For these latitudes, the activated ice number concentration is determined by the temperature-dependent parameterisation described in Section 3.4 and as seen in Figure 5.1. The exponential fit of the data excludes the outlier described in Section 3.4.

4.4 Data postprocessing

The first three months of the simulations are discarded for all experiments, as this is the usual spin-up time for the atmospheric model. In addition,

some combined data variables are created based on the model output. The cloud radiative effect (CRE) at surface for shortwave (SW) and longwave (LW) radiation is calculated as

$$SW_{CRE,surface} = SW_{net,surface} - SW_{clearsky,surface} \tag{4.1}$$
$$LW_{CRE,surface} = LW_{clearsky,surface} - LW_{net,surface} \tag{4.2}$$

following Lamb et al., 2011. The variable "Average ice number concentration in cold clouds" is created by dividing the average ice number concentration by the fractional occurence of ice wherever the latter variable is above zero, and setting "Average ice number concentration in cold clouds" to zero elsewhere. The cloud longwave emissivity (CLWE) is calculating based on the total grid-box cloud liquid water path (CLWP) as

$$CLWE = 1 - \exp(-k \times CLWP) \tag{4.3}$$

following Stephens (2003), where k is the mass absorption coefficient. We use $k = 0.158$ m^2/g, the standard value found by Stephens (1978).

4.5 Spatial and temporal averages

When computing averages over different regions of the model output, differences in the horizontal grid box area of each data point is accounted for by weighting the data points with the cosine of the radian value of the latitudinal degree of each data point, using the `weighted`- and `mean`-functions of the `Python` package `xarray`. The locations of areas where spatial averages were performed can be seen in Figure 4.1. The temporal averages by season or years were done using `xarray`'s `groupby`- and `mean`-function.

4.6 Cloud phase metrics and CALIOP LiDAR comparison

In order to compare the output of our model experiments directly with LiDAR observations, we use the same method as Shaw et al. (2022) to generate output of supercooled liquid fraction (SLF) for two cloud phase metrics, one for "cloud top" and one for "cloud bulk". These are generated by filtering the overlying cloud optical thickness (COT), first by discarding the uppermost layers with COT < 0.3 to avoid including cirrus clouds and then selecting the highest layer of mixed-phase clouds, which is categorised as "cloud top". Second, the "cloud bulk" is acquired by selecting all cloud layers with $0.3 <$ COT < 3.0. The LiDAR observations are from NASA's Cloud-Aerosol LiDAR with Orthogonal Polarization (CALIOP) (Winker et al., 2009). The instrument can discriminate spherical water droplets from non-spherical ice crystals in clouds by the ratio of the perpendicular and parallel backscatter returns from its laser signal. We use CALIOP data averaged over the observational period 2009-06-01−2013-05-31. The observations are binned down to a $1° \times 1°$ resolution for comparison with the model output. The SLF is calculated on isotherms from -40°C to 0°C, with a 5°C increment. The observed SLF is calculated as the the ratio of the number of liquid cloud top pixels to the sum of ice plus liquid cloud top pixels, following Bruno et al. (2021). The modelled SLF is calculated as the ratio of cloud liquid surface area density to the sum of liquid and ice surface area densities, based

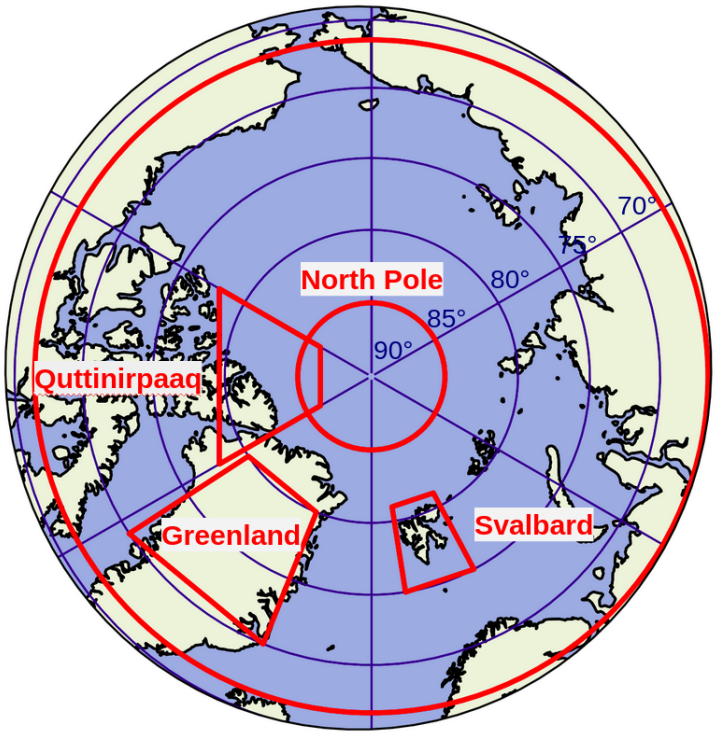

Figure 4.1: The areas used for spatial averaging, marked with red figures.

on the method of Tan et al. (2016), using ratios between cloud ice and cloud liquid mixing ratios. The data is spatially averaged over the Arctic, weighted as described in Section 4.5, for latitude above 66.5° and up to 82°, which is the northernmost limit of the LiDAR observations.

PART III

Results

CHAPTER 5

Observational results

In this chapter the main findings from the field measurements conducted for the purpose of this thesis are presented. In Section 5.1, an overview of all ice nucleating particle (INP) measurements at Andenes are shown, as well as the parameterisations based on the observations. In Section 5.2 the relationship between the INPs and various ambient factors are discussed. In Section 5.3, the ice nucleating ability of the local sea water compared to its total organic carbon (TOC) content is described.

5.1 Characterisation of INP concentrations at Andenes

All measurements of ambient INP concentrations can be seen in Figure 5.1. The concentrations span two orders of magnitude at -15°C, and range between 10^{-4} and 10^{-3} INP/L_{std} to 10^{-2} and 10^{-1} INP/L_{std} within the temperature range investigated. An outlier measurement, marked with green in Figure 5.1 shows considerably higher values, with concentrations almost two orders of magnitude higher than the average concentrations. This measurement somewhat skews the average, as can be seen from the small difference between the parameterisation of INP concentration as a function of temperature of all measurements (orange line) and the parameterisation excluding the outlier (black line). An analogous INP study of Li et al. (2022), conducted at Ny-Ålesund (78°55'N, 11°56'E) in autumn 2019 and spring 2020, show similar concentrations compared to our study at Andenes, with slightly lower values for higher temperatures. This indicates that our measurements are fairly representative for Arctic conditions in spring. From Figure 5.1 it can also be seen that the parameterisation of Meyers et al. (1992), which represents global deposition/condensation freezing in NorESM2, has almost two orders of magnitude higher concentrations than our measurements at the lowest temperatures and four orders of magnitude higher at the highest temperatures. Although our measurements are representative of immersion freezing and not deposition or condensation, it has been shown that immersion freezing is the most relevant pathway for ice formation in high-latitude mixed-phase clouds (Boer et al., 2011; Westbrook et al., 2013). This indicates that primary ice nucleation is highly overestimated in the Arctic mixed-phase clouds of NorESM2 with CAM5 heterogeneus ice nucleation, compared to observations in spring.

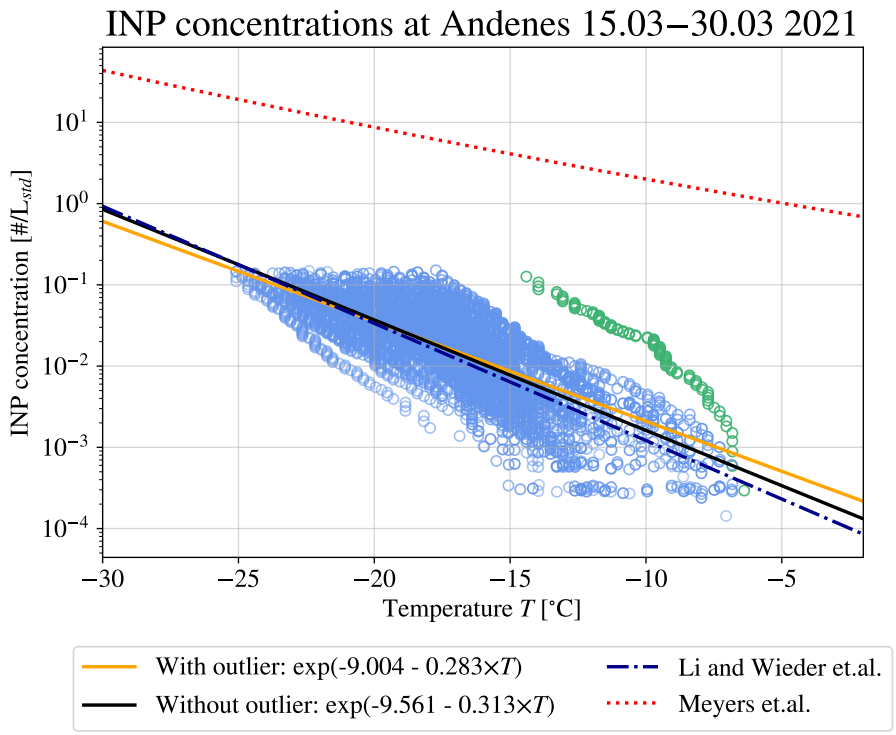

Figure 5.1: All ice nucleating particle (INP) concentrations measured from the air at Andenes in 2021. The measurements are shown with blue and green circles. The green circles are an outlier believed to be influenced by strong southerly winds. The orange line is the parameterisation of INP concentrations as a function of temperature including all measurements ($R^2 = 0.53$), while the black line represents the parameterisation excluding the outlier ($R^2 = 0.59$). For comparison, the INP study of Li et al., 2022 from Ny-Ålesund is included, as well as the parameterisation of Meyers et al., 1992 used in NorESM2.

5.2 INPs and influencing environmental factors

A timeline of our INP measurements is shown as boxplots for freezing temperatures of sampled INPs in Figure 5.2a. Below, they are compared with timelines of environmental factors that could possibly influence the ambient INP concentrations (5.2b-5.2e). More specifically, higher aerosol concentrations of a larger diameter (≥ 0.5 μm) could entail more available particles for ice nucleation as found by DeMott et al. (2010). Greater wind speed could lead to more particles being lofted into the air, as e.g. observed by Inoue et al. (2021) for INP concentrations over ocean. The INP concentration and characteristics could change depending on the different INP source regions (e.g. ocean, bare ground, forest) the air has passed on its way (Wex et al., 2019). Marine biological activity in the nearby sea water could entail higher emissions of biological particles, and thereby INPs, from the ocean, and the sea water TOC concentration could be a relevant proxy for this biological activity (Wilson et al., 2015; McCluskey et al., 2018). As the processes determining INP concentrations are a complex

composition of many factors, we do not expect to find a strong relationship between any of the individual above-mentioned factors and the INP freezing temperatures. The relationships are investigated by averaging each ambient variable over each INP sampling period, the result of which is marked with orange dots for each timeline, and comparing these to the temperature at which 50 % of the aliquots of each INP sample was frozen (hereafter: frozen fraction). The frozen fraction at a given temperature is directly related to the estimation of INP concentrations at that temperature, as described in Section 3.3. The 50 % frozen fraction temperature can therefore tell us at what temperature there is a certain abundance of INPs in sample, which relates both to the general INP concentration and the characteristic freezing temperatures of the present INPs. This comparison can be seen for each ambient variable in Figure 5.2g to Figure 5.2j.

One of the most notable findings is that the ambient concentration of aerosols $\geq 0.5\mu$m does not explain the variability of 50 % frozen fraction temperature of the INPs at all (Figure 5.2g; $R = 0.19; R^2 = 0.03$). This is contrary to previous studies, e.g. by DeMott et al. (2010), and suggests that our INPs measurements could be dependent on smaller particles or on a subset of particles with diameter $\geq 0.5\mu$m that do not covary with the overall concentration of larger particles. The correlation between total aerosol surface area and INP freezing temperatures shows a similar correlation ($R = 0.20; R^2 = 0.04$) and can be found in Appendix A, Figure A.1. A possible explanation for this lack of correlation could be that a portion of the INPs originate from smaller biological fragments, perhaps associated with marine organic aerosols, that does not covary with the total aerosol surface area and concentration of aerosols $\geq 0.5\mu$m.

The strongest relationship is found between the wind speed and the INP 50 % frozen fraction temperatures (Figure 5.2h), where the Pearson correlation coefficient is $R = 0.52$ and $R^2 = 0.27$. As the wind speed is likely to affect other environmental factors as well, most notably the concentration of aerosols $\geq 0.5\mu$m, an investigation of this relationship is also included in Figure 5.2f. The wind speed has similar correlation with the general aerosol concentration as with the INP concentration, with $R = 0.48$. This suggests that both the aerosols $\geq 0.5\mu$m and the INPs could be affected by the wind speed in a similar fashion, but that there are other factors determining both variables so that they become quite independent of each other.

The relationship of wind direction and INPs is investigated by grouping the temperatures at 50 % frozen fraction based on the direction from where the wind originates. The wind directions are grouped by "Arctic" (300°-45°), "Southwesterly" (210°-300°), "Southerly" (175°-210°) and "Easterly" (45°-175°) origin, as can be seen in Figure 5.2i. While both "Arctic" and "Southwesterly" winds come from marine environments, "Southerly" winds travel over the land areas of Andøy, and "Easterly" winds come from the Norwegian mainland, travelling over sea to Andøy before reaching our study area. From Figure 5.2i we can see that the measurements with "Arctic" and "Southwesterly" origin winds generally have higher average freezing temperatures (closer to -16°C) than "Southerly" and "Easterly", even though the latter ones have larger spreads. This could be an indication that INPs from a marine environment

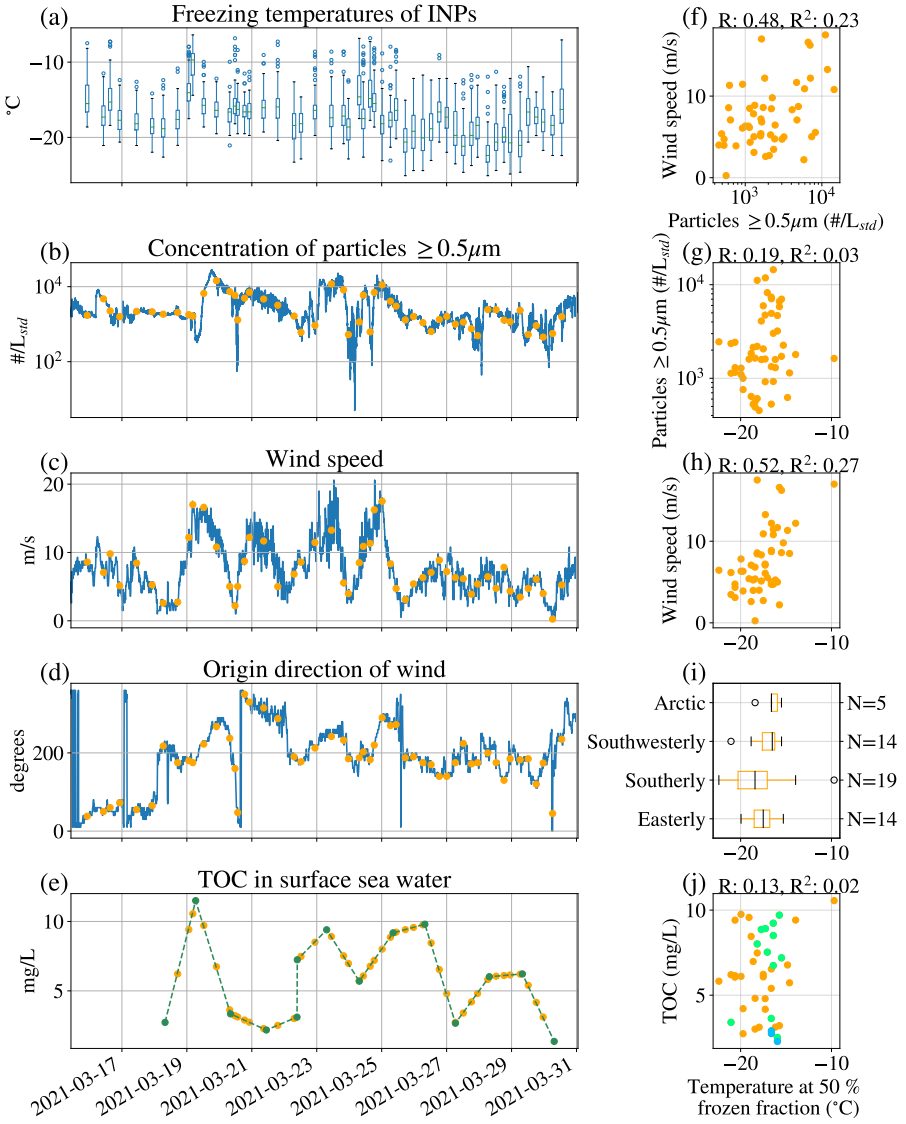

Figure 5.2: Freezing temperatures of all INP measurements in Andenes 2021 (a), compared with simultaneous measurements of ambient aerosols with diameter $\geq 0.5\mu$m (b), wind speed (c) and direction (d) and total organic carbon (TOC) in the surface sea water at the adjacent shore (e). The TOC is linearly interpolated between measurements (green dots). The orange dots in (b)-(e) show the the average values over the INP sampling period, which are used for relationship estimates between the temperature at 50 % frozen fraction in air and the other variables in (g)-(j). The green (blue) dots in figure (j) shows measurements at a time when the wind was of Southwesterly (Arctic) origin. A strength-of-relationship estimate for wind and aerosols $\geq 0.5\mu$m can also be seen in (f).

consist of more biological INPs, that typically have higher freezing temperatures than e.g. dust aerosols, while winds that travels over land contain INPs from

a larger variety of sources, such as dust, vegetation or pollution. It should be noted, however, that the "Arctic" sample size consists only of five measurements, and should not be considered statistically meaningful.

The variability of INPs does not seem to be explained by the TOC content in the adjacent sea water, with $R^2 = 0.02$ (Figure 5.2j). The first high peak in TOC on March 19th (Figure 5.2e) does correspond with the outlier value of the INP measurements from the same time (Figure 5.2a), lending further evidence to the possibility that organics-rich sea spray was entering the measuring inlet at the time due to southerly winds colliding with waves. All measurements considered, the correlation is $R = 0.13$, but increases slightly if we only consider measurements corresponding to "Southwesterly" wind origin from marine environments (green dots in Figure 5.2j). The correlation is then $R = 0.28$ ($R^2 = 0.08$). The measurements corresponding to "Arctic" wind origin (blue dots in Figure 5.2j) only have a sample size of three, and is not considered here. It is important to note, however, that the TOC measurements only have a daily resolution and therefore, a major portion of the TOC values are linearly interpolated to match the INP sample periods. This could lead to a misrepresentation of the relationship between TOC and INP concentrations. In addition, it is also worth considering that the TOC in the adjacent shore might not be representative of potential biological sources farther out at sea where the air masses originate.

5.3 Sea water TOC and ice nucleation

If TOC is indeed a good proxy for INP-relevant biological activity in the ocean, we would expect the ice nucleating ability of the sea water itself to correlate positively with the TOC concentrations of the water. The relationship between the TOC content of sea water and the corresponding temperature at 50 % frozen fraction of the sea water can be found in Figure 5.3a. The figure includes both the sea water samples from the shore adjacent to the study area (green dots) and samples taken from the open sea at the east side of Andøy (turquoise dots). However, we do not find a clear relationship in our measurements. The correlation is a negative one, with a Pearson correlation coefficient of -0.21 for all samples combined and with $R^2 = 0.05$.

Previous studies have investigated the ice nucleating properties of sea water in relation to its total carbon content. Wilson et al. (2015) found the sea surface microlayer (SML; $\sim$ 1 to 1000 μm in thickness) to consistently freeze at higher temperatures than subsurface water, relating this to the distinct biological properties of the SML and amongst others, its organic carbon content. They developed a parameterisation (hereafter: W15) based on their measurements for the cumulative number of INPs per gram of TOC for the SML as a function of temperature. They found that their measurements fell within one order of magnitude of their parameterisation. As our measurements show a poor relationship between TOC and INP freezing temperatures, we do not make an analogue parameterisation here, but our measured values of cumulative INPs per gram of TOC can be found in Figure 5.3b, with W15 for comparison. Most of our measurements actually do fall within $\pm$ one order of magnitude of the W15 (marked with dashed red lines). The rest of the measurements fall

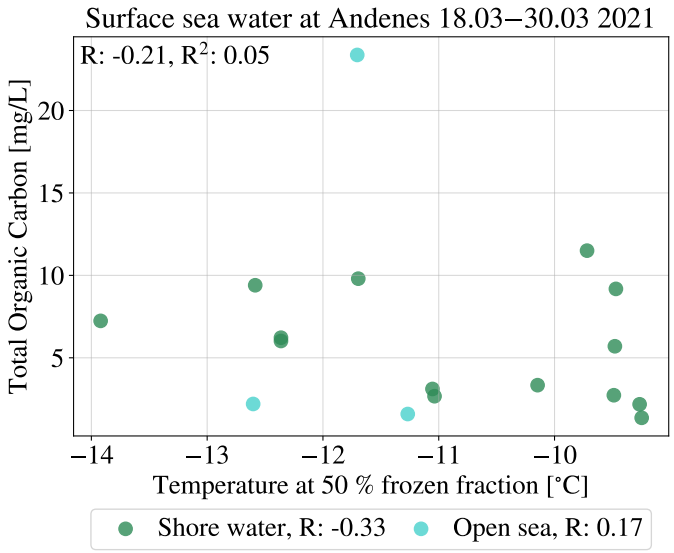

(a)

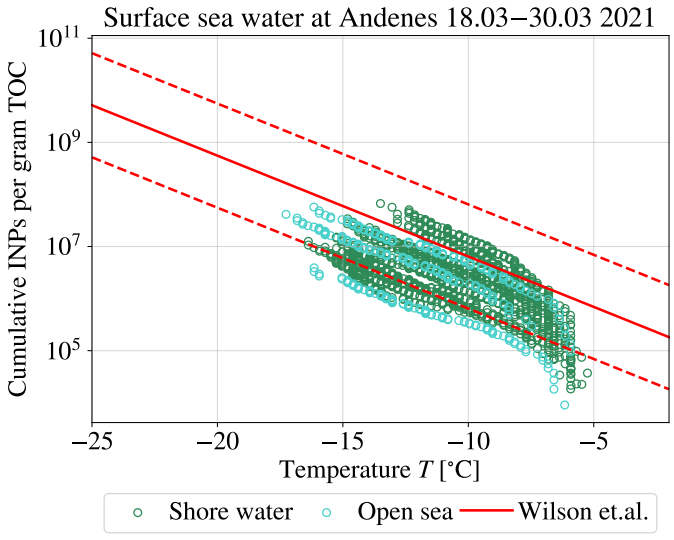

(b)

Figure 5.3: The relationship between the temperature corresponding to 50 % activated INPs and the TOC in sea samples (a) and the cumulative concentration of INPs in the ocean per gram TOC (b). The green dots mark samples from the study area shore, and the turquoise dots mark samples from the open sea on the east side of Andøy, and the red line marks the paremterisation of Wilson et al., 2015, with ± 1 order of magnitude (dashed lines). R corresponds to the Pearson correlation coefficient.

below, and the average values are also lower than W15. This can possibly be explained by the fact that our measurements include 1-2 cm of the sea surface layer, not only the SML, and therefore could contain more of the less INP-rich subsurface water. In addition, the close proximity to the shoreline from where many of the samples were conducted may cause more mixing and a less intact SML. Studies investigating the relationship between total organic concentrations of marine INPs with the INP efficiency (McCluskey et al., 2017; McCluskey et al., 2018) have also found lower INP concentration per gram of TOC than W15. A possible explanation presented by McCluskey et al. (2017) is that the complex process of bubble bursting leading to emissions of marine aerosols entrains some bulk sea water, entailing a mix of particles from both the SML and the underlying surface water in the marine aerosol concentration. Irish et al. (2019), on the other hand, found that INP concentrations predicted from the ice nucleating properties of the SML underestimated the field measurements of marine organic aerosols of e.g. DeMott et al. (2016). This underlines the importance of understanding the emission processes of biological material to the atmosphere in order to relate TOC in sea water to INPs in the air, as done in Figure 5.2j.

CHAPTER 6

Modelling results

In this chapter the main findings from the modelling portion of this thesis are presented. These include how aligning modelled Arctic INP concentrations with observations from Andenes in 2021 affects the NorESM2 simulation with CAM5 heterogeneous ice nucleation. The differences between the heterogeneous ice nucleation microphysics in CAM5 and CAM6 for selected variables can be found in Appendix A. Here, the changes related to cloud phase and how these compare to LiDAR observations are described in Section 6.1, and then the cloud cover changes are presented in Section 6.2. Lastly, the changes in cloud radiative effects and their implications for surface temperature are presented in Section 6.3.

6.1 Cloud phase changes

The direct effect of the parameterisation adjustment in "Andenes 2021" compared to "CAM5" can be seen in Figure 6.1. The figure shows the average activated ice number concentration due to the parameterisation of Meyers et al. (1992) (used in "CAM5") and the adjusted parameterisation in "Andenes 2021", as a function of height. Averaging over the simulation period and the Arctic (left plot), we see that the parameterisation adjustment has the highest impact at the 900 hPa level, which corresponds to the low cloud regime. Here, the change in activated ice number concentration is around two orders of magnitude, decreasing from between 0.1 and 1 activated ice particles/L to between 0.001 and 0.01 activated ice particles/L. The difference between the two parameterisations decreases with decreasing pressure and temperature, as expected from Figure 5.1 and, more importantly, from the fact that neither parameterisations are active at temperatures below -37°C. When examining the spatial change at the 859 hPa level (right plot), we see that the relative change in activated ice crystal number concentration is rather uniform across the Arctic. The average Arctic decrease at this height level is -98.9 %. The lowest relative change can be seen over Greenland, corresponding to between -95 % and -90 %. Here, the elevation and subsequently lower temperatures over Greenland could explain why the parameterisation adjustment has less relative impact over Greenland than over other areas.

In Figure 6.2a and Figure 6.2b we see the effect this parameterisation adjustment has on average ice number concentration in cold clouds and the grid box averaged

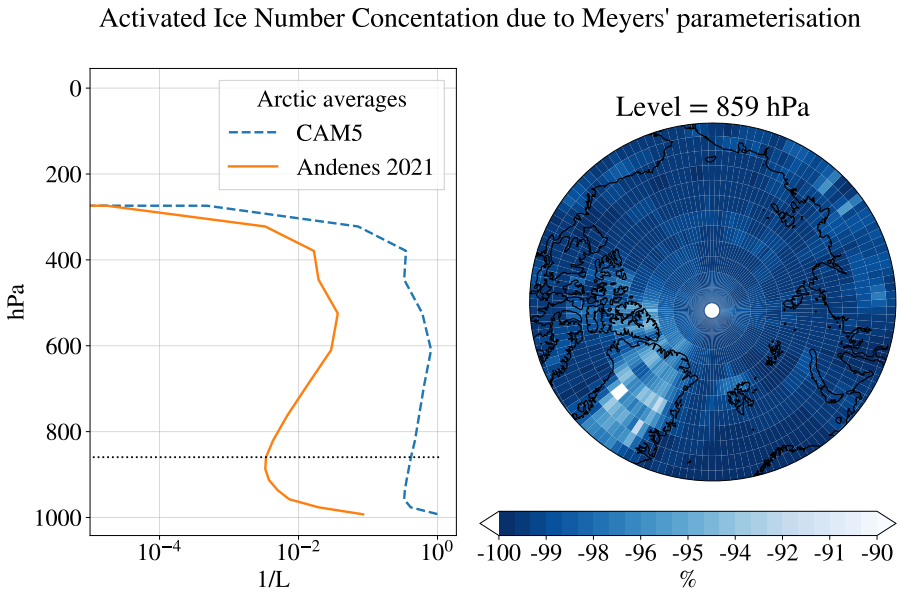

Figure 6.1: The activated ice number concentration due to the parameterisation of Meyers et al., 1992 in "CAM5" and for the adjusted parameterisation in "Andenes 2021", averaged over the period 2007-04-15 to 2010-03-15. Left: the average values over all latitudes above 66.5°N for height levels in hybrid sigma pressure coordinates (midpoint). Right: the relative change from "CAM5" to "Andenes 2021" at pressure level 859 hPa. The level is marked with a black dotted line in the left plot.

cloud ice amount, respectively. First and foremost, we see that there is a general reduction in both ice number concentrations in cold clouds and cloud ice amount throughout the Arctic region. However, there are also some slight positive changes in Figure 6.2a (right plot), and the magnitude of the decrease is generally lower than in Figure 6.2b. This is likely due to the fact that the cold cloud average ice number concentration is a combined variable, consisting of the average cloud ice number concentration divided by the fractional occurrence of ice, and that we also generally see decreases in the fractional of ice clouds (see Figure A.2b in Appendix A). If we consider the average cloud ice number concentration separately (see Figure A.2a in Appendix A), the relative changes are strictly negative. The largest decreases in cold cloud average ice number corresponds well with where the largest decreases in averaged cloud ice amount are, except for over Greenland. Here, the averaged cloud ice amount change is lower than at similar latitudes, and closer to the smaller relative changes we see in the central Arctic. This is expected, as the temperatures in these areas are somewhat lower than elsewhere, allowing more ice to form in the clouds even with the adjusted parameterisation. The reason why we see relatively large decreases in cold cloud average ice number concentration over Greenland is therefore due to the increases in the fractional occurrence of ice clouds in these areas (see Figure A.2b). This could again be explained by changes in the cloud fraction itself, which is further investigated in Section 6.2.

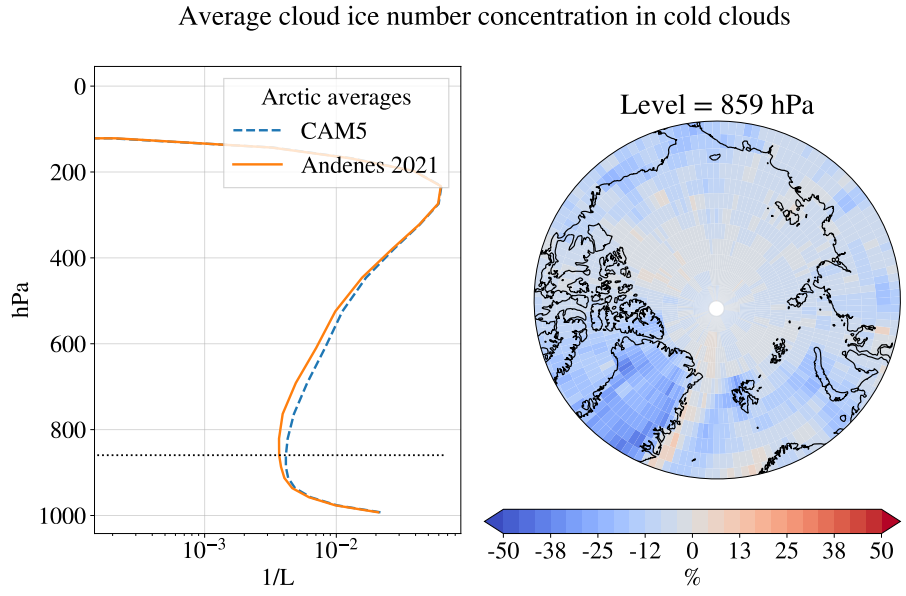

(a)

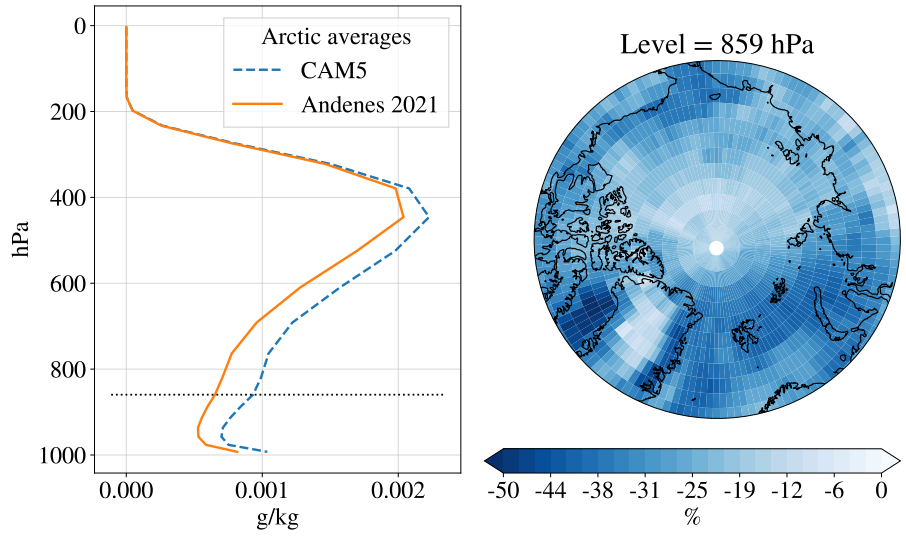

(b)

Figure 6.2: The average cloud ice number concentration in cold clouds (a) and grid box averaged cloud ice amount (b) for "CAM5" and "Andenes 2021", averaged over the period 2007-04-15 to 2010-03-15. Left: the average values over all latitudes above 66.5°N for height levels in hybrid sigma pressure coordinates (midpoint). Right: the relative change from "CAM5" to "Andenes 2021" at pressure level 859 hPa. The level is marked with a black dotted line in the left plot.

Further, we can see the total grid-box cloud ice water path (CIWP) change in Figure 6.3 and the total grid-box cloud liquid water path (CLWP) change in Figure 6.4, separated by season. Here the changes are shown in absolute numbers in order to compare more directly with the absolute changes in cloud radiative effect in Section 6.3. The relative changes for selected areas in CIWP and CLWP can be found on the right side plot in Figure 6.5a and Figure 6.5b, respectively.

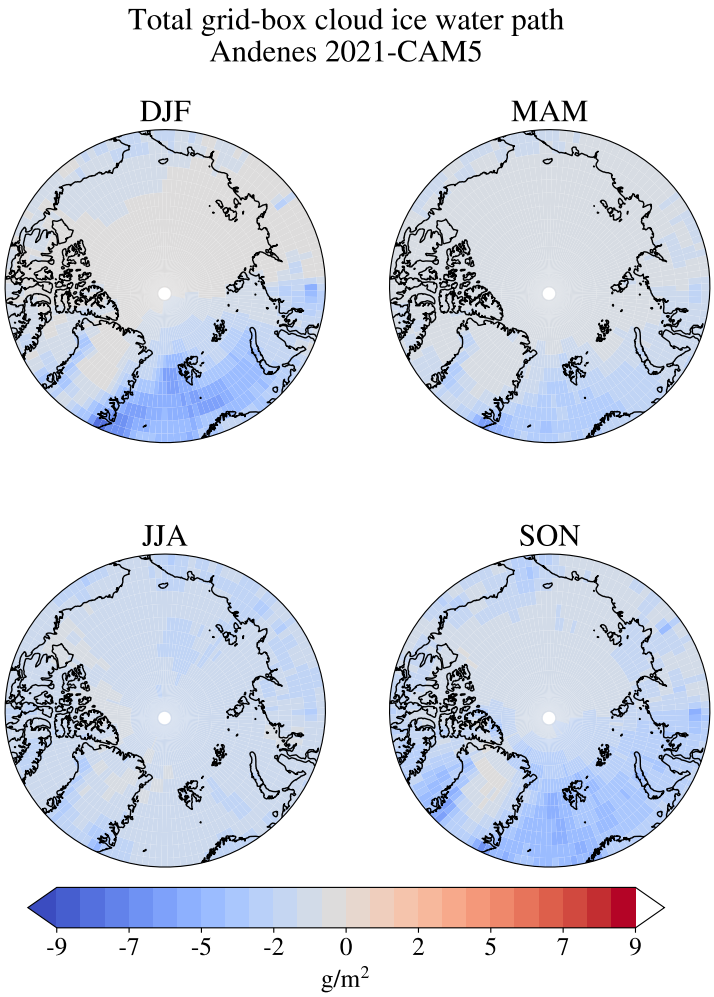

Figure 6.3: The seasonal change in total grid-box cloud ice water path between "Andenes 2021" and "CAM5", averaged over the period 2007-04-15 to 2010-03-15. Negative values correspond to lower cloud ice water path in "Andenes 2021" compared to "CAM5".

The strongest decrease in CIWP happens over the Norwegian sea, including Svalbard, in winter, spring and autumn (see Figure 6.3; Figure 6.5a). In summer, the decrease is quite uniform over the whole Arctic, but of a slightly lower magnitude. For the Arctic in general, the largest decrease in CIWP appears in autumn, as can also be seen from the blue line in Figure 6.5a. The average

relative change in the whole Arctic is around -14 %, with the highest relative change happening over Svalbard.

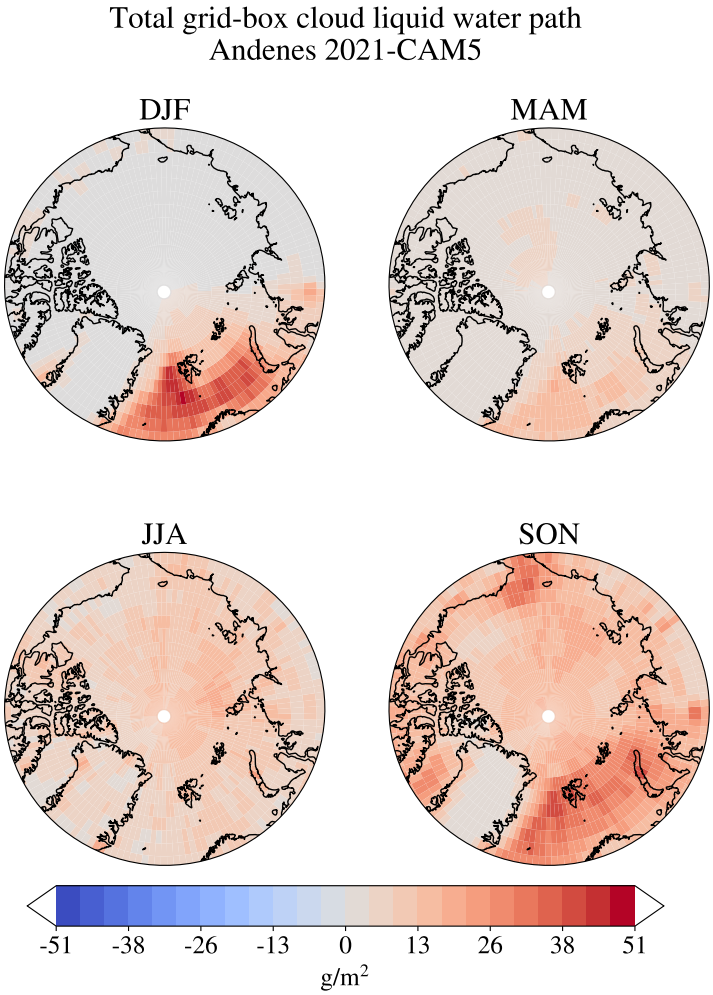

Figure 6.4: The seasonal change in total grid-box cloud liquid water path between "Andenes 2021" and "CAM5", averaged over the period 2007-04-15 to 2010-03-15. Positive values correspond to higher cloud ice water path in "Andenes 2021" compared to "CAM5".

The CLWP changes (see Figure 6.4; Figure 6.5b) follow a similar spatial pattern as the CIWP changes, except that where we see a decrease in CIWP we see an increase in CLWP, with a much larger magnitude. For example, the decrease of around 4 g/m^3 in CIWP that we see over Svalbard in October in Figure 6.5a corresponds to an increase of 40 g/m^3 in CLWP in Figure 6.5b. The average relative increase in CLWP over the Arctic is around 65 %.

This large difference in magnitude could be explained by the Wegener–Bergeron–Findeisen (WBF) process (Storelvmo et al., 2015), described in Section 2.2. The rapid growth of ice crystals can cause the clouds to dissipate

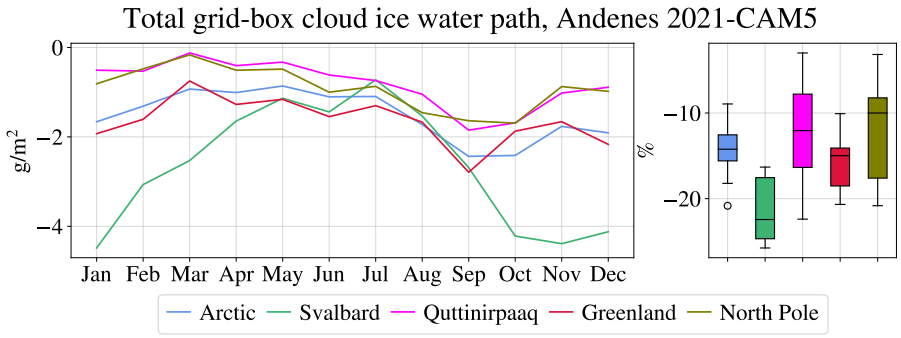

(a)

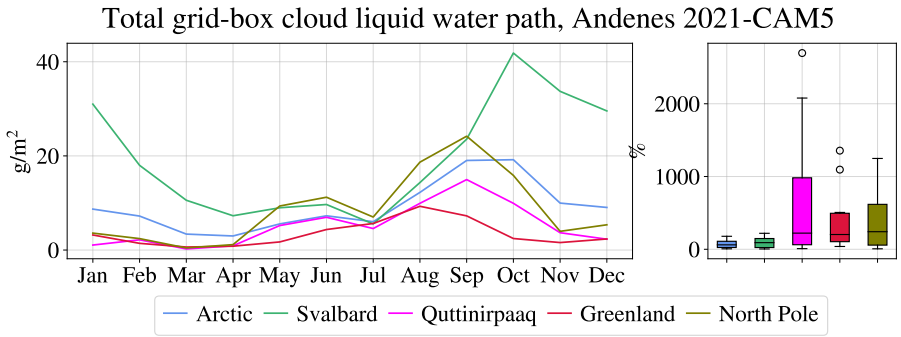

(b)

Figure 6.5: The change in total grid-box cloud ice water path (a) and total grid-box cloud liquid water path (b) between "Andenes 2021" and "CAM5", averaged over the period 2007-04-15 to 2010-03-15. Left: absolute change for each month averaged over selected regions. Right: the distribution of relative change over the months in the same regions.

faster, as the particles reach a large enough size to fall out from the cloud at a quicker rate than through the growth of liquid particles. A significant reduction in ice particles can contribute to a reduction in the efficiency of the WBF process, and thereby lead to a liquid water content in the clouds much higher than the reduction in ice content itself, as the liquid water is no longer changing phase and precipitating out of the cloud at the same rate. We can see that the peaks in CIWP change and CLWP change in Figure 6.5a and Figure 6.5b, respectively, do not always match, which could be explained by seasonal variations in the strength of this process. Interestingly, we see that while the relative change in CIWP was largest over Svalbard in Figure 6.5a, the largest relative changes in CLWP are over Quttinirpaaq, Greenland and the North Pole, where we see extremely large relative changes, reaching over a 1000 % change or more in some seasons. These are places with very low CLWP in CAM5, causing the change in CLWP in "Andenes 2021" to make a relatively larger impact than over Svalbard, even though the absolute change is much higher here.

In order to see how the changes in modelled cloud phase due to the parameterisation adjustment compares to actual observations, a comparison

between the supercooled liquid fraction (SLF) for each cloud isotherm in the model and in CALIPSO LiDAR observations is included in Figure 6.6.

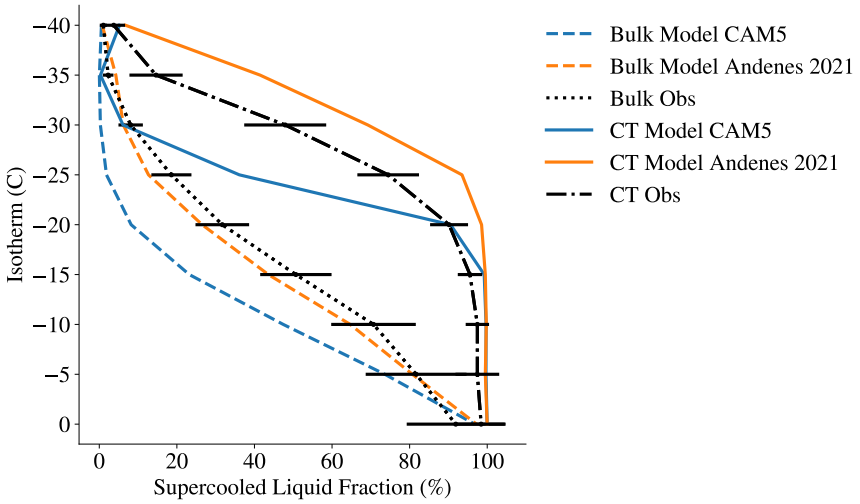

Figure 6.6: The supercooled liquid fraction for each isotherm in clouds for latitudes above 66.6°N and below 82°N. The dashed lines show the relationship for bulk cloud in the modelled climate, and the solid lines show the relationship for cloud top (CT) in the modelled climate, both in "CAM5" (blue) and "Andenes 2021" (orange), averaged over the period 2007-04-15 to 2010-03-15. The black dotted line shows the relationship for the bulk cloud as observed by the CALIOP LiDAR, while the dashdotted line shows the same for cloud top, averaged over the period 2009-06-01 to 2013-05-31. The error bars correspond to one standard deviation in the LiDAR measurements.

For the bulk of the cloud, the parameterisation adjustment in "Andenes 2021" shows SLFs much closer to the observations than "CAM5". "CAM5" shows around 20 % lower SLF for temperatures between -10°C and -25°C. "Andenes 2021" reduces this gap to around 5 % less SLF compared to observations, with slightly higher SLFs at temperatures higher than -5°C and less than -35°C. However, virtually all "Andenes 2021" SLF values fall within the uncertainty of the LiDAR measurements. For cloud top, the "Andenes 2021" experiment overestimates the SLFs for temperatures < -15°C. The SLF remains close to 100 % at cloud top for temperatures down to -25°C, whereas the observations show a larger decrease in SLF at these temperatures, with 80 % SLF at -25°C. "Andenes 2021" overestimates the SLF by around 20 % at lower temperatures, approaching 30 % at -35°C, before becoming closer to the observations again. This could be an indication that the adjusted parameterisation is most representative for lower altitudes, but that would not explain the slight underestimation for SLF in cloud bulk. Another explanation could be that ice crystals could be falling from the cloud top to the interior of the cloud too fast in the model. "CAM5", on the other hand, generally underestimates the cloud top SLF. Down to around -20°C the modelled SLF follows the observations quite well, but here they diverge from the observations and show SLFs around 40 % less than the observations at

temperatures down to -30°C. At lower temperatures, the "CAM5" simulation begins to approach the observations again, underestimating the SLF by only 10 % at -35 °C, and shows an unexpected increase in SLF at -40 °C, which might be an artefact of the binning of isotherms in the model. Overall, the "Andenes 2021" improves the SLFs in Arctic clouds, performing best for bulk cloud and coming closer to observations at cloud top, despite the overestimation in cloud top SLF at cold temperatures. This supports that representing heterogeneous ice nucleation in Arctic mixed-phased clouds more realistically in models is an important step towards more realistic modelling of Arctic cloud phase, but that there are other processes for cloud ice formation that may not yet be fully captured. These could be attributed to ice crystal sedimentation or secondary ice production, described in Section 2.2.

6.2 Cloud cover changes

When considering the cloud cover differences averaged over the Arctic and the entire modelling period in Figure 6.7 (left), the differences between "CAM5" and "Andenes 2021" are rather small. The same is true for the differences in seasonal cloud cover between the parameterisations, as can be seen in Figure 6.8. There is some spatial variation in the relative cloud cover changes at 859 hPa (hybrid sigma pressure coordinates) in Figure 6.7 (right).

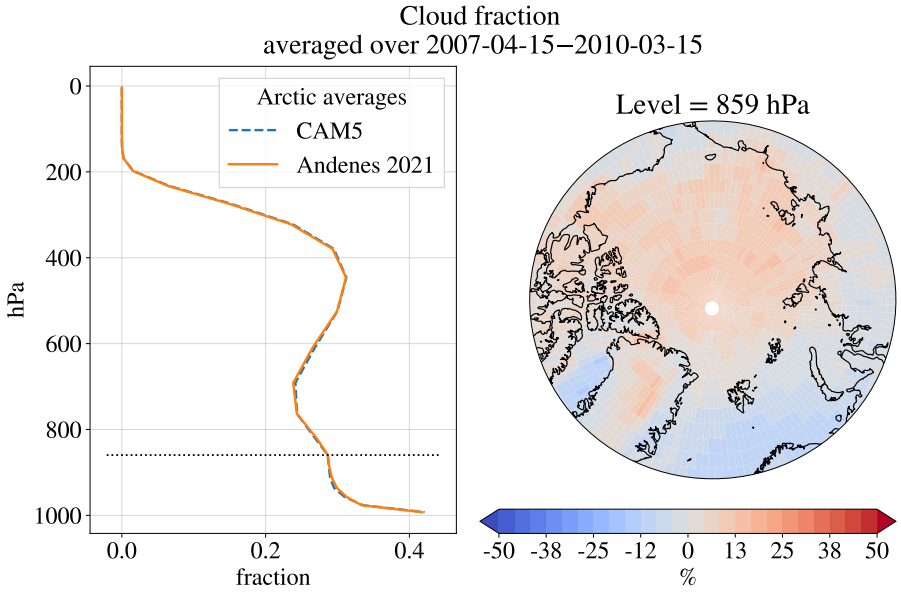

Figure 6.7: The cloud fraction for "CAM5" and "Andenes 2021", averaged over the period 2007-04-15 to 2010-03-15. Left: the average values over all latitudes above 66.5°N for height levels in hybrid sigma pressure coordinates (midpoint). Right: the relative change from "CAM5" to "Andenes 2021" at pressure level 859 hPa. The level is marked with a black dotted line in the left plot.

Most notably, we see a small increase of between 10 % and 15 % over Greenland and areas that mainly correspond to sea ice covered ocean. Over the Norwegian

sea and the Baffin bay, we see a decrease in cloud cover of approximately the same magnitude. The fact that we see an increase in clouds over Greenland is consistent with the increase in simulated fractional occurrence of ice clouds there, leading to the relatively large decrease in average ice number concentration in this area found in Figure 6.2a. The increase in fractional occurrence of ice clouds could be explained simply by there being more clouds that contain ice, but with lower ice number concentrations than before. What is interesting to note is that we also observe a large increase in clouds over the sea ice-covered Arctic, but without a similar effect of increased fractional occurrence of ice. This would suggest that most of the increased cloud cover here is due to more warm clouds, not ice clouds. These are also areas where we see a very large relative change in CLWP (see Figure 6.5b), which supports this hypothesis.

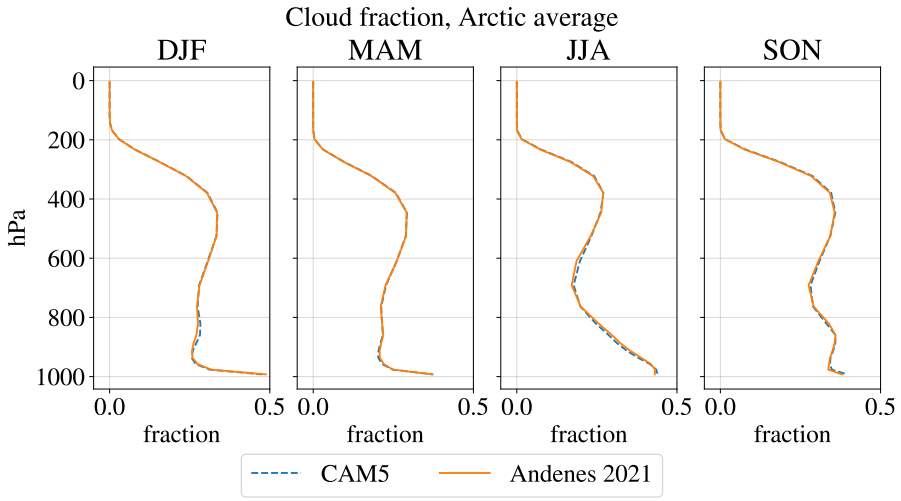

Figure 6.8: The seasonal cloud fraction for "CAM5" and "Andenes 2021", averaged over the period 2007-04-15 to 2010-03-15 and over all latitudes above 66.5°N, for height levels in hybrid sigma pressure coordinates (midpoint).

The cloud lifetime, which is important for the cloud cover, is largely influenced by the cloud phase partitioning of the clouds. With more liquid clouds the cloud lifetime should increase, and so an increase in cloud cover is expected. From Figure 6.8 we see that cloud fractions at lower levels generally have a slight increase over the entire Arctic, even though the changes are small. The fact that the design of our model simulation prevents us from seeing the full response of the climate to the parameterisation change, makes the cloud cover changes difficult to interpret. However, as we can see in Figure 6.9a and Figure 6.9b, the parameterisation adjustment generally has a more visible impact on the change in the ice liquid water mixing ratio in clouds than the cloud cover itself. It is therefore the decrease of cloud ice content and the corresponding increase in cloud liquid content we attribute most explanatory power when considering changes to the cloud radiative effects, as discussed in Section 6.3.

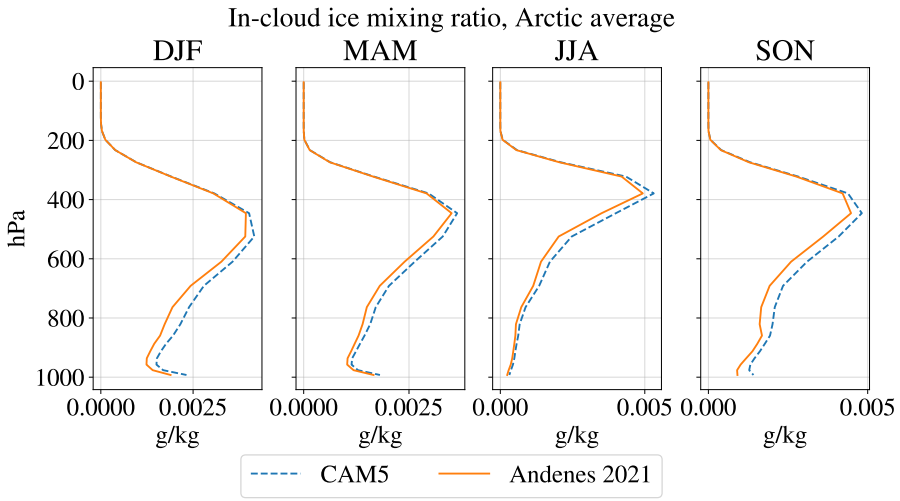

(a)

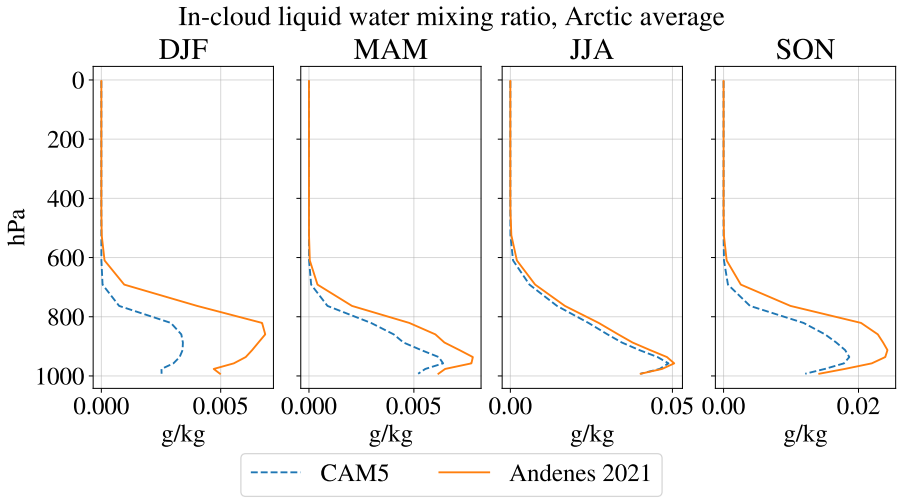

(b)

Figure 6.9: The seasonal in-cloud ice water mixing ratio (a) and in-cloud liquid water mixing ratio (b) for "CAM5" and "Andenes 2021", averaged over the period 2007-04-15 to 2010-03-15 and over all latitudes above 66.5°N, for height levels in hybrid sigma pressure coordinates (midpoint). Note that the x-axes have different values to capture variations in different seasons.

6.3 Cloud radiative effect changes

The seasonal change in shortwave cloud radiative effect at the surface between "Andenes 2021" and "CAM5" across the Arctic can be seen in Figure 6.10.

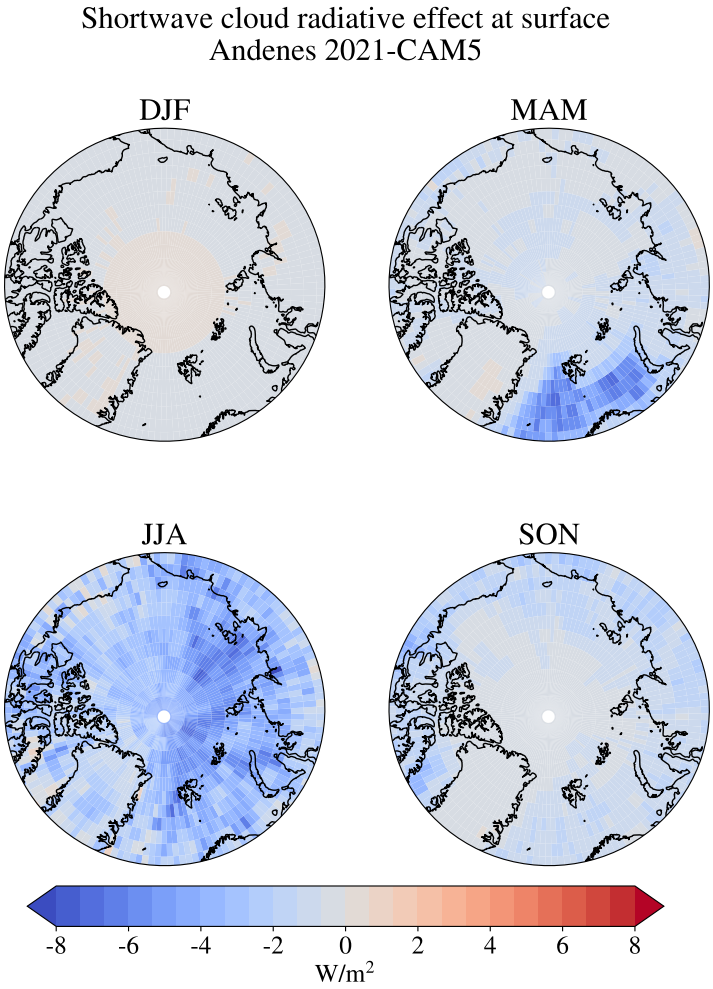

Figure 6.10: The seasonal change in shortwave cloud radiative effect at the surface between "Andenes 2021" and "CAM5", averaged over the period 2007-04-15 to 2010-03-15. Negative values correspond to less incoming solar radiation due to clouds in "Andenes 2021" compared to "CAM5".

The change is largely dependent on the solar zenith angle, giving large absolute values during the sun-rich summer and late spring months, and close to zero changes for the winter months and at latitudes above 80° in autumn. In summer, the change ranges from 2 to 8 W/m^2 less incoming solar radiation in "Andenes 2021" over the entire Arctic, consistent with the pattern change in summer CLWP seen in Figure 6.4. The average change across the Arctic is around -3 W/m^2 in summer, which can be seen from Figure 6.13a. In spring, the largest change is located over the Norwegian sea, with values between -5

and -8 W/m^2. This is also the region where we find the largest increase in spring CLWP. In autumn, the change is around -1 to -2 W/m^2 at latitudes below 80° and Greenland, where the change is close to zero. This corresponds well with the distribution of CLWP change as well, taking into account that there is much less solar radiation in autumn than in spring and summer and a significantly lower increase in CLWP over Greenland in autumn compared to the rest of the Arctic in "Andenes 2021". These changes culminate in an average relative change in shortwave cloud radiative effect at the surface across the Arctic of around -15 % (Figure 6.13a).

The seasonal change in longwave cloud radiative effect at the surface between "Andenes 2021" and "CAM5" across the Arctic is seen in Figure 6.11.

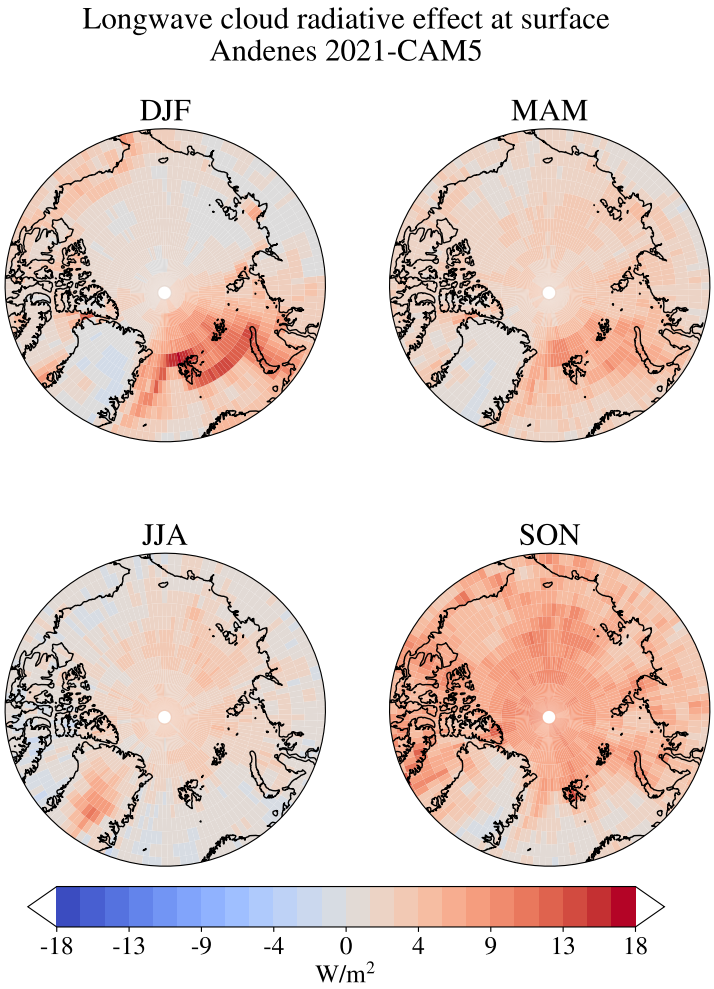

Figure 6.11: The seasonal change in longwave cloud radiative effect at the surface between "Andenes 2021" and "CAM5", averaged over the period 2007-04-15 to 2010-03-15. Positive values correspond to less outgoing longwave radiation due to clouds in "Andenes 2021" compared to "CAM5".

As described in Section 2.3, the increase in the longwave cloud radiative effect due to increased CLWP is non-linear, as opposed to the shortwave cloud radiative effect. The longwave cloud radiative effect is dependent on the cloud longwave emissivity, which can be highly sensitive to changes in CLWP if it increases from previously small values, but insensitive if the previous value were large. An estimation of the change in estimated cloud longwave emissivity resulting from the CLWP changes can be found in Figure 6.12. Taking the latter into account, the changes in longwave cloud radiative effect at the surface can largely be explained by the changes in CLWP as well. The estimated cloud longwave emissivity in "Andenes 2021" can be found in Figure A.3 in Appendix A.

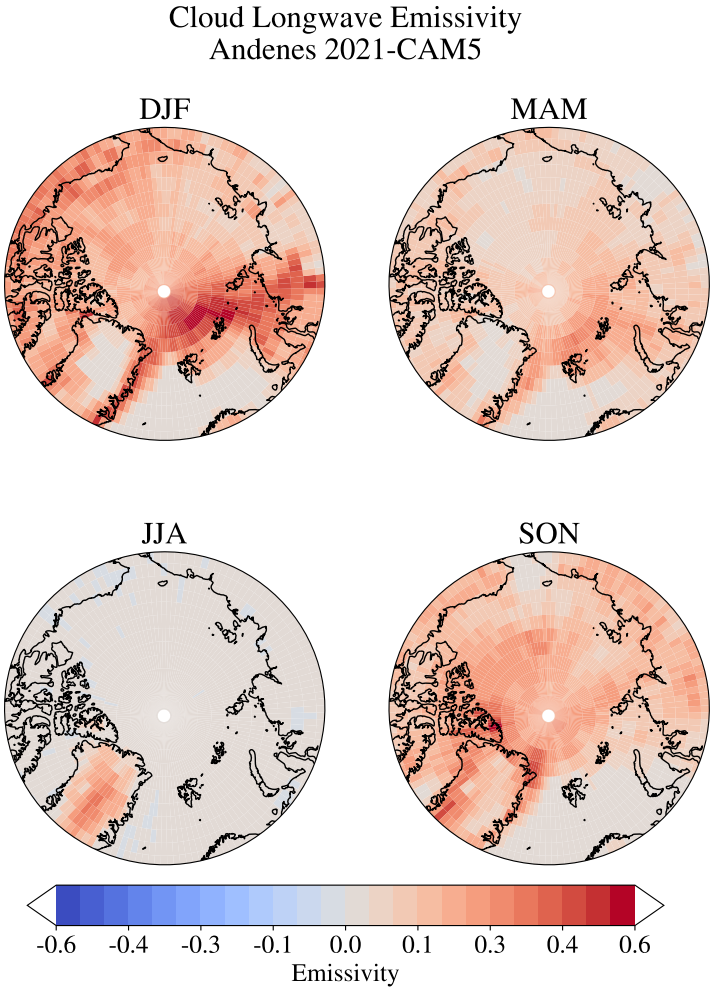

Figure 6.12: The seasonal change in estimated cloud longwave emissivity between "Andenes 2021" and "CAM5", averaged over the period 2007-04-15 to 2010-03-15. Positive values correspond to higher longwave emissivity of clouds in "Andenes 2021" compared to "CAM5".

In the winter months, the largest increases in longwave cloud radiative effect

can be found along the ice edge west, north and east of Svalbard, with values approaching 10 to 15 W/m^2. The increase in this area is even more pronounced than the changes we see in cloud longwave emissivity (Figure 6.12) in this area compared to the rest of the Arctic. This is likely due to the fact that this area is cloudier than the rest of the Arctic, making it more affected by the emissivity change. In spring, the increase in longwave cloud radiative effect is strongest north and east of Svalbard, which is also where we see the strongest changes in cloud longwave emissivity. It is interesting to note that we observe little change in longwave cloud radiative effect over the Norwegian sea, even though the change in shortwave cloud radiative effect is between -5 and -8 W/m^2 here in spring. This can be explained by the clouds in this area already containing a fair amount of liquid water, so the resulting change in CLWP makes little difference to the cloud longwave emissivity (Figure 6.12). In summer, what stands out is the comparatively large increase of longwave cloud radiative effect, between 5 and 10 W/m^2, over Greenland. This corresponds to a large increase in cloud longwave emissivity, which is absent for the rest of the Arctic. The small increases in longwave cloud radiative effect we see over the sea ice covered Arctic might result from the general increase in low-level clouds (Figure 6.7; Figure 6.8). In autumn, the increase is large (between 5 and 10 W/m^2) over the entire Arctic, except for over the Norwegian sea and parts of Greenland, where the CLWP increase is low (Figure 6.4).

The total relative change in longwave cloud radiative effect across the Arctic is around 15 % , as seen in Figure 6.13b. On Svalbard, the changes are largest in winter, while Quttinirpaaq and the North Pole, as well as the Arctic in general, show the largest changes in autumn, as well as a minor peak in spring. While the magnitude of change is largest on Svalbard, approaching 15 W/m^2 increased longwave cloud radiative effect in December, the average relative changes are largest over Quttinirpaag and the North Pole.

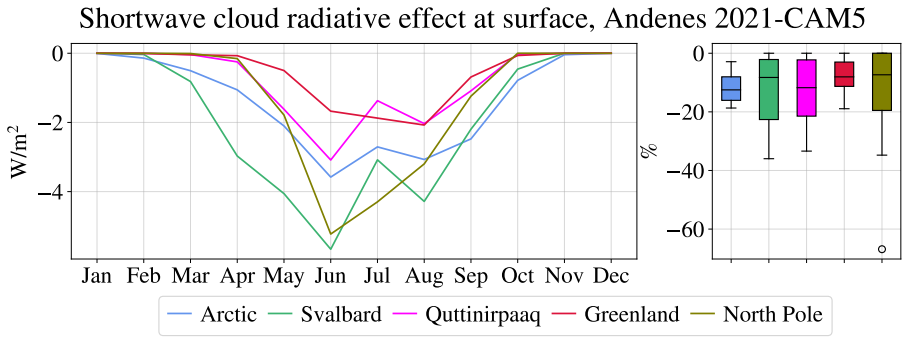

(a)

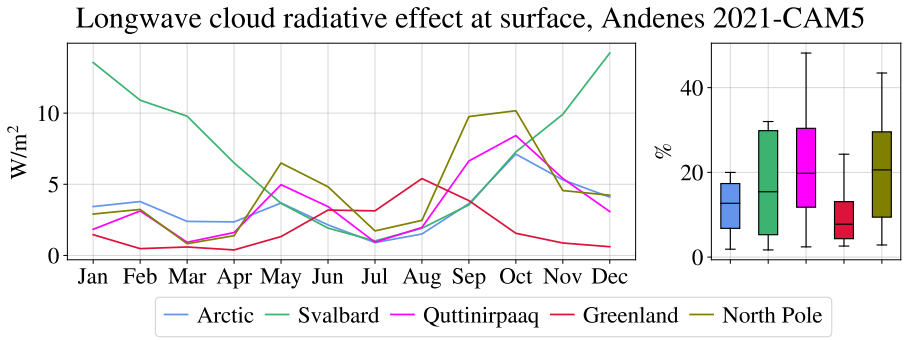

(b)

Figure 6.13: The change in shortwave cloud radiative effect (a) and longwave cloud radiative effect (b) between "Andenes 2021" and "CAM5", averaged over the period 2007-04-15 to 2010-03-15. Left: absolute change for each month averaged over selected regions. Right: the distribution of relative change over the months in the same regions.

To give an indication of the implications of these changes in cloud radiative effects, the seasonal changes in surface temperature between "CAM5" and "Andenes 2021" across the Arctic domain are included in Figure 6.14. It should be stressed that the surface temperature changes shown here are not representative of the full response to the radiation changes, as the sea surface temperatures are fixed in the model. I will therefore not focus on temperature changes over open ocean, and it should be noted that the temperature changes over land and sea ice will also be muted due to the fixed sea surface temperatures. With the exception of Greenland, there is an overall increase in temperature in winter, spring and autumn, with the strongest changes in winter and autumn. In winter, the increase approaches 1°C or more north and east of Svalbard and over the island itself. In autumn, the increase is most pronounced in the central Arctic, where competing effects from decreased shortwave radiation are smaller due to little incoming solar radiation. The temperature increase in winter is more evenly distributed than the increased winter longwave cloud radiative effect, which is likely a result of temperature changes being effectively distributed throughout the Arctic by the general circulation. However, it could be an indication that the temperature increase in winter is also a result of built

up heat from autumn. In spring, the temperature increase is slightly lower, likely due to more built up heat having been lost during winter and competing shortwave cloud radiative effects. In summer, these shortwave effects result in largely unchanged temperatures across the Arctic. The exceptions are Siberia, where the shortwave cloud radiative effect surpasses the longwave one, resulting in a summer temperature decrease, and Greenland, were the increased summer longwave cloud radiative effect dominates the shortwave one, resulting in a temperature increase in this area. It should be mentioned that as Greenland and sea ice covered areas already have a high albedo, an increase in cloud albedo has little chance of decreasing the general shortwave effect enough to make up for increases in longwave cloud radiative effect (Zhang et al., 1996).

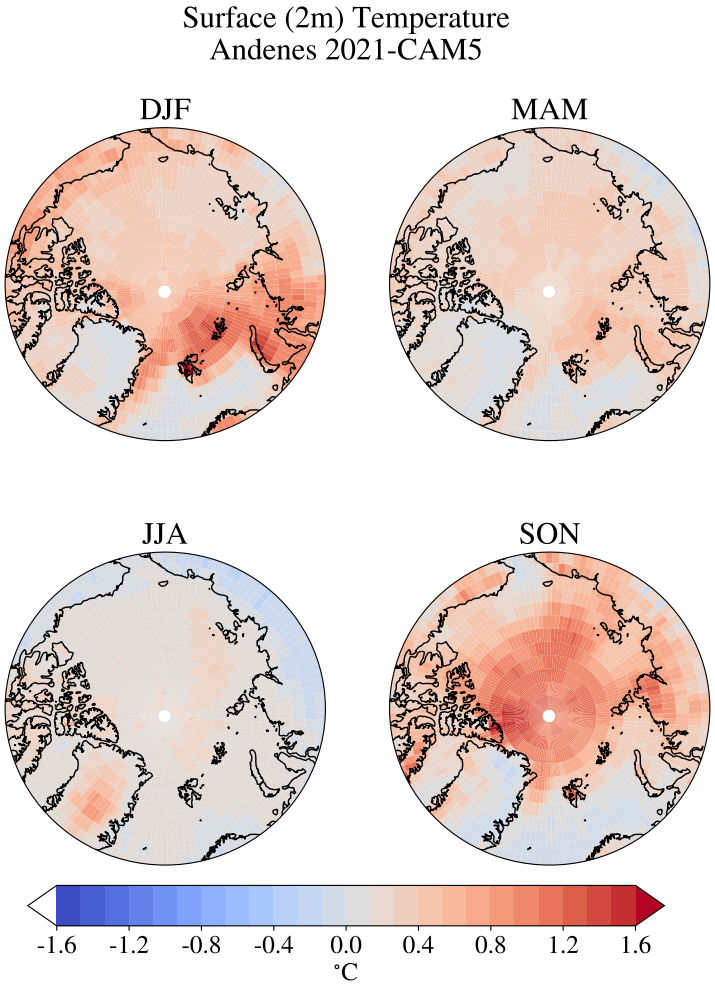

Figure 6.14: The seasonal change in surface temperature between "Andenes 2021" and "CAM5", averaged over the period 2007-04-15 to 2010-03-15. Higher temperatures correspond to a temperature increase in "Andenes 2021" compared to "CAM5".

The net change in the cloud radiative effect and the change in surface

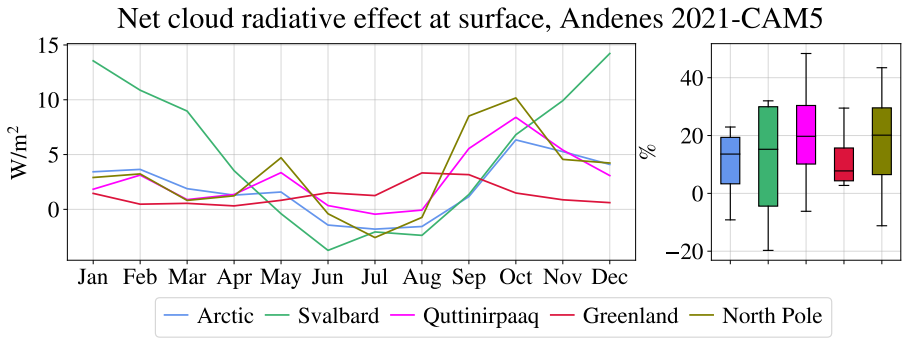

(a)

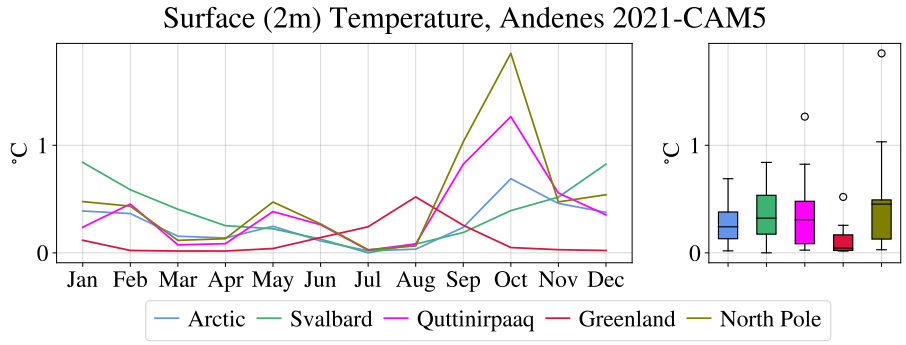

(b)

Figure 6.15: The change in net cloud radiative effect (a) and surface temperature (b) between "Andenes 2021" and "CAM5", averaged over the period 2007-04-15 to 2010-03-15. Left: absolute change for each month averaged over selected regions. Right: the distribution of relative change (a) and absolute change (b) over the months in the same regions.

temperatures for selected areas, is seen in Figure 6.15a and Figure 6.15b, respectively. The effect of the parameterisation adjustment is an average relative increase of net cloud radiative effect of around 15 %. The largest magnitude of this change is found in October, with an increase of 6 W/m^2. Overall, this leads to an average annual increase in Arctic temperatures of 0.3°C, highest in October with 0.7°C. However, it is important to note that these temperature changes might be modest by design, due to the fixed sea surface temperatures. Over Svalbard we see a 0.4°C average change, and we see the highest temperature average change over the North Pole of 0.5°C. There are in addition large peaks in temperature changes of between 1 and 2°C over the central Arctic in autumn.

PART IV

Discussion and Conclusion

CHAPTER 7

Discussion

The results in this thesis are discussed in this chapter, beginning with a discussion of how representative the INP measurements themselves are in Section 7.1 and how representative the model parameterisation is in Section 7.2. Further, the implications of this study for our understanding of Arctic climate change are discussed in Section 7.3. Finally, a discussion of how both the observational and modelling work in this thesis can contribute to future INP modelling is discussed in Section 7.4.

7.1 The representativeness of the INP measurements

The INP measurements in this thesis were only conducted at a single site and over a short period of time. This requires careful consideration of how representative they really are for the entire Arctic and over the whole year, which is what they are used for in the modelling work.

First, these INP measurements are from Andenes (Norway) which climatically is not representative of the entire Arctic. The Norwegian island is surrounded by open sea throughout the year, which is possibly a source of marine organic INPs (Wilson et al., 2015) that sea ice covered regions and inland areas lack. Indeed, there is space-borne evidence that sea ice cover could inhibit the availability of INPs (Carlsen et al., 2022). In addition, Andenes is located at 69°N, which is at the southern edge of where the parameterisation is applied. The more southern Arctic latitudes have a closer proximity to INP sources more characteristic of lower latitudes, such as dust, vegetation and anthropogenic emissions, which might cause INP concentrations to be higher at the southern edges of the Arctic. The measurements were deliberately taken at a time of frequent cold air outbreaks (CAOs), which are inclusions of polar air masses into ice-free regions. These CAOs are usually most prevalent during boreal spring, when the polar jet surrounding the Arctic during the sharp winter temperature gradient begin to weaken. The similarity between our measurements and the measurements of Li et al. (2022), taken at Ny-Ålesund (seen in Figure 5.1), suggests that the campaign was successful in capturing polar air masses. However, as Ny-Ålesund is located close to the ice-free Fram strait, this area is likely not representative of the Arctic as a whole either. It is important to note that the modelling study in this thesis is to be interpreted first and foremost as a sensitivity study of the model climate to an adjusted

INP parameterisation. Though we likely expect air masses closer to the Arctic to be even more pristine, this mainly entails that we can consider our INP measurements as an upper limit to what we might expect to be realistic in the Arctic at the time of our measurements.

Second, our measurements were only conducted at the surface level. The parameterisation based on these measurements is applied to the entire air column with temperature lower than -37°C, but is not necessarily representative at higher levels of the troposphere. Since the Arctic is characterised by a relatively low, stable boundary layer, we expect most of the INPs measured at the surface to be an upper limit of the concentrations for the entire air column if the relevant INP sources are mostly emitted at the surface (Griesche et al., 2021). However, we cannot rule out the potential for elevated plumes of dust or pollution being transported from lower latitudes above the boundary layer, making the air here less pristine than at the surface, as found to be important by e.g. Schrod et al. (2017), and Marinou et al. (2019) in other areas. This represents an uncertainty in the representativeness of the INP measurements for the entire column. However, Arctic clouds are typically quite low, and much of the cloud cover forms close to the boundary layer, which is an argument for surface INP concentrations being representative for most Arctic clouds (Griesche et al., 2021).

Third, the measurements were only conducted during March of 2021. There could be considerable interannual variability, and perhaps even more seasonal variability, due to environmental factors such as snow cover and biological activity. Less snow cover and stronger biological activity would likely lead to increased INP sources in boreal summer (Creamean et al., 2019; Wex et al., 2019; Tobo et al., 2019). We therefore assume our INP measurements to be an underestimation of INP concentrations in summer and perhaps also early autumn. In summer, the main impact of this underestimation would entail an overestimation of the cloud liquid water path (CLWP) in the model, meaning less decrease in shortwave cloud radiative effect and thereby less cooling in summer. The increase in longwave cloud radiative effect could also be overestimated in early autumn. It is difficult to speculate whether these measurements would be an underestimation during summer and early autumn for the whole Arctic, as we additionally expect areas such as the central Arctic and Greenland to be more pristine than Andøy. This underlines the need for more spatially and seasonally diverse Arctic INP measurements. However, an informed guess would be that the introduction of a seasonally dependent INP parameterisation mainly would contribute to less surface cooling from liquid clouds in summer, thereby leading to an overall warmer present day simulated climate.

7.2 The representativeness of the INP parameterisation

The way we implement these INP measurements through a parameterisation of immersion freezing INP concentrations as a function of temperature deserves a discussion of how representative it truly is of the physical processes it is supposed to represent. Even though temperature definitively is the clearest

predictor of our measured INP concentrations compared to other predictors we have considered, such as aerosols $\geq$ 0.5 μm and wind seen in Figure 5.2, predicting the INP concentrations by temperature alone is obviously a clear simplification. Many of the complex mechanisms leading to spatial and temporal variability are excluded, such as differences in sources and sinks, recycling, chemical aging and in-cloud physical modification of INPs (Kanji et al., 2017). As touched upon in Section 4.2, our INP parameterisation is just one of many different parameterisation types. It does not consider the size or composition of aerosols or the time they are exposed to a certain temperature and supersaturation over ice, as opposed to many time-dependent INP parameterisations based on classical nucleation theory (CNT) (e.g. Hoose et al., 2010). It is important to be aware that our parameterisation has these simplifications, but the argument for using it is that other current INP parameterisations also do not capture all relevant physical processes. CNT-based parameterisations have e.g. been shown not to reproduce the temperature dependence of immersion freezing (Kanji et al., 2017), which is important based on our measurements. It should also be considered that our measurements are only valid between -6 and -25°C (see Figure 5.1), but that we extrapolate down to -37°C and up to values close to 0°C using exponential fitting. This is due to the fact that our measurement technique does not allow us to measure INP concentrations at temperatures below -25°C, as the purified water we use (see Section 3.2) freezes above the homogeneous freezing temperature. This extrapolation might therefore not be representative, especially for lower temperatures. It does, however, show close similarity to the parameterisation of Li et al. (2022), which is based on measurements at temperatures down to -30°C.

One way of evaluating the representativeness of the INP parameterisation is to compare the modelling results with observations, as we have done in Figure 6.6. However, doing so requires caution. Similarities between observations and models could arise for the wrong reasons, i.e. due to compensating factors and not because the parameterisation is more representative of the relevant physical processes. In addition, when comparing the model experiments to the LiDAR observations, it should be noted that the time periods of comparison are different. This should not make too much of a difference, considering that supercooled liquid fractions (SLFs) for each isotherm do not show much seasonal variability (Hofer, 2022, personal communication), due to which we do not expect much interannual variability either. More importantly, the way the SLFs are retrieved for the cloud top and the cloud bulk is defined by thresholds for optical thickness (Shaw et al., 2022), and due to the difference in vertical resolution in the LiDAR and model data, the model SLF is from deeper bin sizes. It should also be noted that LiDAR and model comparison does not provide any indication of representativeness for latitudes above 82°, as LiDAR observations for this area are not available.

As stated in Section 6.1, the parameterisation adjustment shows an overall improvement of SLFs for each isotherm, but with an overestimation of SLF at cloud top. The discrepancies could be due to the representativeness of the parameterisation itself, the representativeness of the measurements and poor representation of other processes important for ice formation in the model. This is in addition to the above-mentioned factors influencing the

comparability between observations and model experiments. It should also be mentioned that as the surface warms slightly with the parameterisation change, the isotherms could shift slightly and not correspond to the same cloud height levels for the different model experiments. To cite Otto (2012): "The modeller knows which part of the climate system is deliberately poorly represented, but what he does not know is which other processes are affected by this simplification" (p. 51). As previously stated, the extrapolation of our INP parameterisation to warmer and colder temperatures could be unrepresentative, which could explain the overestimation of SLF for cloud bulk at the lowest and highest temperatures seen in Figure 6.6. The reason why we see a slight underestimation of SLF for the intermediate temperatures could be because the parameterised INP concentrations are slightly too high for most of the Arctic, owing to the measurements themselves not being representative enough. As the SLFs all fall within the uncertainty of the LiDAR measurements, these differences are of little significance. It is however important to note that the close similarity we see for modelled and observed cloud bulk is not necessarily due to the modelled heterogeneous ice nucleation being close to the actual one. The results could be hiding a larger discrepancy between ice nucleation in the real and modelled world, that is compensated by other real-world processes not well captured by the model, such as secondary ice production. For the cloud top, the overestimation of SLF could indicate that the measurements are not representative of the whole column, and that the modelled INP concentration therefore is too low for higher altitudes. However, it could also be due to processes not captured by the simplified parameterisation, such as preactivation of INPs (Kanji et al., 2017) on their ascent to the cloud top. To summarize, the adjustment of this parameterisation seems to overall improve the representation of ice content in Arctic clouds, as we would expect from the fact that it is based on observations from the Arctic, but there are many questions left to answer when it comes to how closely it represents Arctic ice nucleation.

7.3 The implications for Arctic climate

Regardless of how well the parameterisation represents Arctic immersion freezing, it is possible to discuss the implications it has for modelled Arctic climate. The reduction in heterogeneous ice nucleation in the adjusted parameterisation leads to a large increase in cloud liquid water path (CLWP). We find that the main implications of this is a large increase in longwave cloud radiative effect at the surface, especially in autumn and winter, which leads to an average increase in surface temperatures. Since the sea surface temperatures are fixed, the temperature increase would almost certainly be even higher if the ocean surface could respond to the cloud and subsequent radiation changes. If we assume that the adjusted parameterisation is closer to the real world than the standard CAM5 physics, based on the larger discrepancy between "CAM5" and observations in SLF, this entails that the present Arctic climate modelled by CAM5 has a surface temperature contribution from clouds that is too low.

The discrepancy in surface temperature contribution from clouds in the different parameterisations could have multiple implications if the climate warms. As the modelling study in this thesis does not include investigations of

global warming, reasoning about the effect of an adjusted parameterisation in a warmer climate should be considered speculative. Assuming that increased temperatures would entail less activated INPs, we would likely see a further increase in CLWP with warming. As our findings show that the increase in longwave cloud radiative effect at the surface (a positive feedback on temperature) dominates the decrease in shortwave cloud radiative effect at the surface (a negative feedback) when CLWP increases, this would suggest that surface temperatures would increase further if the climate warms. In that case, the cloud phase of Arctic clouds would constitute a positive climate feedback contributing to Arctic amplification, consistent with the findings of Tan et al. (2019).

We found that our parameterisation increased the net radiative cloud effect at the surface by around 15 % for an increase in CLWP of around 65 % in the Arctic. We do not know what the additional increase in CLWP could be in a warmer climate − this depends not only on the number of activated INPs and the Wegener–Bergeron–Findeisen (WBF) process, but also on overall changes in cloud formation. However, we also do not know if increases in CLWP would affect the surface net radiative cloud effect similarly as observed with the adjusted parameterisation in present day climate. As described in Section 2.3, the increase in surface longwave cloud radiative effect can be large if CLWP increases from low levels, but if the longwave emissivity of the cloud is already close to 1, an increase in CLWP does not increase the surface longwave cloud radiative effect. This could be described as a "longwave saturation" of the clouds. The surface shortwave cloud radiative effect, on the other hand, could still increase. Due to this phenomenon, the increase of surface net cloud radiative effect with CLWP could be less in a warming scenario than what we see when we adjust the parameterisation. The effect that cloud lifetime could have on longwave radiative effect also plays into the uncertainty, but generally this means we could expect the surface warming of the Arctic under increased temperatures to be less with the adjusted parameterisation than with the standard CAM5 physics. Whether the amplifying effect of increased CLWP will be largest in "Andenes 2021" or "CAM5" depends on how close the clouds are to reaching "longwave saturation" in present day climate, and to what extent CLWP will be increased with temperatures for both parameterisations. The former we can speculate in by considering the estimated cloud longwave emissivity with the adjusted parameterisation can be found in Figure A.3 in Appendix A. It shows that the clouds are already somewhat close to "longwave saturation" in autumn in the present climate, with an emissivity around 0.6 in sea ice-covered areas. The clouds are, however, less optically thick in winter, spring, and generally over Greenland. Though the adjusted parameterisation gives more "saturated" clouds, there is potential for further increased longwave radiative effect in many areas and seasons with warming. Though these are only speculations, the questions raised here are highly relevant for the future of Arctic climate, and make up important directions for future modelling work, preferably using other models as well.

Even if the INP measurements used for the adjusted parameterisation were to be fairly representative in present Arctic climate, this would not guarantee their representativeness in a warming scenario. A reduction in

sea ice and snow cover with warming could lead to stronger sources of INPs in the Arctic, as indicated by the study of Carlsen et al. (2022). A weaker temperature gradient between the Arctic and lower latitudes could also lead to more intrusions of air with higher INP concentrations. If an increase in CLWP does indeed constitute a positive feedback in the Arctic, higher concentrations of INPs could perhaps dampen it. However, taking into account that the sources might mainly increase during boreal summer, when increase in CLWP mainly contributes to cooling through the negative cloud phase feedback, the increase in INPs could lead to less cooling and perhaps constitute a positive feedback in itself. Accounting for the effects of changes in INP concentrations in a warming climate requires parameterisations that explicitly connect INPs to environmental sources (Murray et al., 2021).

7.4 The implications for INP modelling

One of the important findings in this thesis is that an observation-based adjustment to the Arctic INP parameterisation of NorESM2 does have a considerable impact on the modelled liquid content of clouds and thus, on the Arctic surface radiation budget. This underlines the importance of representing heterogeneous ice nucleation correctly in models, for the Arctic in particular but likely for other areas as well. However, we have also found that it is not straightforward to link INP concentrations to different environmental factors. Contrary to DeMott et al. (2010), we found little relationship between INPs and aerosols with diameter ≥ 0.5 μm (see Figure 5.2), suggesting that the measured Arctic INPs are either dependent on a subset of larger particles, on particles of a smaller size, or on the degree of which these particles contain biological material. A good candidate for such particles could be marine organic aerosols. Turning our attention to a proxy for marine biological activity, total organic carbon (TOC) in sea water, did not produce a clearer picture. The number of cumulative INPs measured for each gram of TOC in sea water was not too far below the measurements of Wilson et al. (2015), but the TOC amount and the freezing temperatures of the INPs in the sea water did not show a clear correspondence. It should be stressed that our sample size only consists of 17 samples, and could be prone to chemical degradation during storage time. Thus, we do not have the grounds to conclude that sea water TOC itself is not a good proxy for INP-relevant ocean biological activity that could be used in future INP parameterisations. However, our findings indicate that there are likely other biological factors apart from simply the TOC itself that determine the ice nucleating ability of the sea water. Previous studies have also shown that the ice nucleating ability of dissolved organic matter (DOM), which makes up a portion of TOC, is very sensitive to photomineralization (Borduas-Dedekind et al., 2019), further questioning the suitability of TOC as straightforward predictor of INPs. The mechanism by which marine biological material is transported to the air is also a complex process involving bubble bursting at the surface (McCluskey et al., 2017), potentially explaining why cumulative INP number per gram of TOC in marine aerosols themselves also show lower values than measured by Wilson et al. (2015) (McCluskey et al., 2018).

There are many uncertainties when it comes to predicting INPs based on a proxy for ocean biological activity such as TOC, and further research is still needed to make physically sound parameterisations for INPs in marine environments. There are many efforts going into this, with some showing promising results, e.g. the study of Zhao et al. (2021). As touched upon in Section 2.4, implementing complex INP parameterisation based on multiple environmental factors comes at a computational cost, potentially at the expense of other important processes. However, the more problematic issue for INP modelling is that no physically-based parameterisation currently exists that can fully capture the INP behaviours observed in different regions and seasons. As long as there is a great deal more research needed to have this in place, simplified parameterisations based on present day observations, such as ours, could be important intermediate solutions to the problems climate models show in reproducing cloud phase. The amount of effort that should be put into implementing more complex INP parameterisations should depend on how important they will likely be in a warming climate, which requires further modelling work. However, the Arctic is warming four times faster than the rest of the world (Rantanen et al., 2021). We are observing climatic changes at an unprecedented pace that could be changing the INP concentrations dramatically from a baseline we do not have full understanding of. The work in this thesis therefore underlines the importance of more observational studies of Arctic INP concentrations and their relations to the environment.

CHAPTER 8

Conclusion

8.1 Summary

This thesis has centered around three main research questions presented in the introduction.

First, we have quantified the ice nucleating particle (INP) concentrations active in the immersion freezing mode in Andenes in March 2021. At -10°C, the concentratation ranged between approximately 0.0003 and 0.005 INPs/L_{std}. At -15°C, we observed concentrations between 0.001 and 0.03 INPs/L_{std}. At -20°C, the concentration ranged between 0.01 and 0.2 INPs/L_{std}. The parameterisation of the concentration as a function of temperature shows close similarity to the measurements of Li et al. (2022), taken at Ny-Ålesund in Fall 2019 and Spring 2020. From this, we can conclude that our measurements seem fairly representative for the polar air masses reaching Andenes in spring through cold air outbreaks. How they compare to INP concentrations in other parts of the Arctic and in other seasons, remains to be investigated.

The relationships between INP concentrations and selected environmental variables have also been explored. Contrary to DeMott et al. (2010), we observed negligible correlations between INP freezing temperatures and the presence of ambient aerosols with diameter ≥ 0.5 μm. From this we conclude that the INPs at Andenes are either dependent on smaller particles, or a subset of particles ≥ 0.5 μm that do not covary with the general aerosol ≥ 0.5 μm concentration. There was a correlation of 0.52 between wind speed and INP freezing temperatures, suggesting that the strength of the wind speed partly contributes to the availability of INPs. Wind directions with origin from marine environments were found to have higher freezing temperatures than those from land environments, which on the other hand had larger spreads. We also found a negligible correlation between the total organic carbon (TOC), a proxy for biological activity that could contribute to INPs (Wilson et al., 2015), in the adjacent shore sea water and freezing temperatures of ambient INPs. It should be stressed that the TOC concentration acquired at the shore may not be the most important contributor to potential biological INPs in the air, compared to biological activity further out at sea, since TOC not relevant for INPs could be accumulated at shore through shore erosion. A comparison with the ice nucleating ability and other properties

of sea water from offshore measurements, as done by e.g. Irish et al. (2019), could perhaps provide a clearer link between INPs and marine biological activity.

Second, the implementation of of an observation-based INP parameterisation for the Arctic in NorESM2 was shown to make a significant impact on the ice and liquid content of low-level Arctic clouds. The total grid-box cloud ice water path (CIWP) was reduced by 15 % over the entire Arctic, the absolute changes being largest in boreal autumn, followed by winter. The total grid-box cloud liquid water path (CLWP) correspondingly increased by 65 % over the entire Arctic, with the absolute changes in autumn of around 20 g/m^2. This led to a significant improvement in modelled supercooled liquid fractions (SLFs) for each cloud isotherm compared to LiDAR observations. The modelled SLFs fell within the uncertainty estimates of the observations for cloud bulk with the adjusted parameterisation, and overestimated them for cloud top.

Third, the same implementation led to increases in longwave cloud radiative effect at surface in autumn, winter and spring due to increased cloud optical thickness that dominated the decrease in shortwave cloud radiative effect at surface in summer. The result led to an average increase in net cloud radiative effect at surface of 15 % over the entire Arctic, with more than a 5 W/m^2 increase in October and November. This produced an overall increase in average surface temperature of 0.3°C−0.5°C, indicating that the present day surface temperature in NorESM2 with the heterogeneous ice nucleation of CAM5 is probably too low. The large increase in surface longwave radiative effect compared to shortwave is likely due the non-linear relationship between cloud longwave emissivity and CLWP, causing the longwave emissivity to increase drastically as the CLWP increased from low values in autumn, winter and spring. The same non-linear relationship could entail that further increases in CLWP with warming may not lead to similar temperature changes. This is because the longwave emissivity might not increase as dramatically with warming as with the parameterisation adjustment, considering that the clouds would already have a higher liquid water content. However, the increase of CLWP in Arctic clouds could still constitute a positive feedback.

8.2 Outlook

There are many possibilities for further work related to this thesis, in addition to the above-mentioned points regarding how the INP measurements compare to other Arctic measurements as well as relevant environmental factors. First, it is of great interest to investigate the effects of the adjusted INP parameterisation in a warming climate. This would provide an indication of how much of a difference it makes for the development of Arctic climate to have modelled heterogeneous ice nucleation more representative of present Arctic observations. Still, this is not enough to answer the more pressing question, which is what role INPs will truly play in future warming of the Arctic. Answering this question requires INP parameterisations that are not only latitude-dependent functions of temperature, such as ours, but ones that are responsive to changes in relevant environmental factors based on physically established relationships. They need to be able to represent seasonal and spatial variations as well as

warming-induced changes to the environment. Predicting the effect INPs will have also depends on being able to represent other relevant cloud microphysical processes, such as secondary ice production, in a satisfactory way. The points below are a non-exhaustive list of research questions that it would be interesting to try to answer in future work:

- How diverse is the seasonal and spatial variation in Arctic INPs, and how do concentrations in remote sea ice- or snow covered areas especially compare with concentrations close to the open ocean or snow-free land?
- How can proxies for marine biological activity be linked to INP concentrations in a physically sound way that is simple enough to be parameterised in a global climate model?
- How would a representative INP parameterisation affect the net cloud radiative effect in the Arctic as well as the rest of the world, in a warming climate?

Answering these questions will be important steps towards a better understanding of the role cold clouds play in global warming and limiting the uncertainty in climate predictions (Prenni et al., 2007; Murray et al., 2021). This will in turn be of utmost importance for society and the pathways that should be taken to stay within a safe operating space for humanity.

Appendices

APPENDIX A

Figures

This appendix includes figures excluded from the main findings. Figure A.1 shows the relationship between INP freezing temperatures and total aerosol surface area. Figure A.2a and Figure A.2b show average cloud ice number concentration and the fractional occurence of ice, respectively, for "CAM5" and "Andenes 2021". Figures A.4a to A.9 show the difference between "CAM6" and "CAM5" for selected variables.

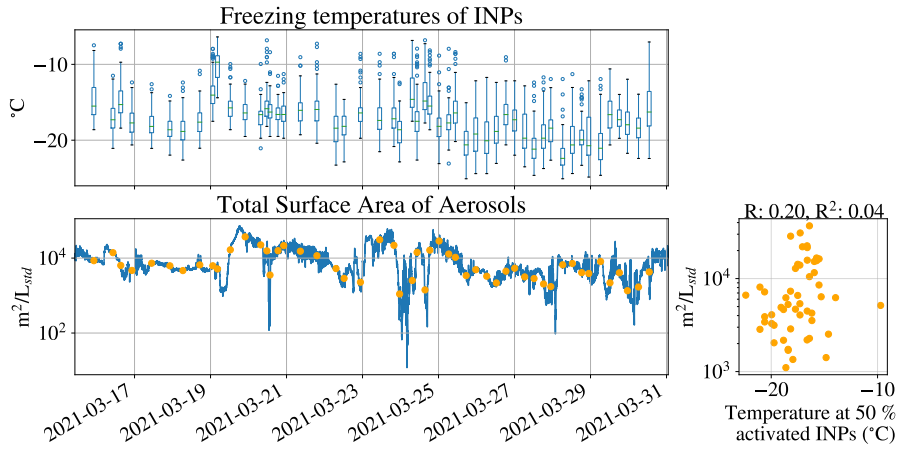

Figure A.1: Freezing temperatures of all INP measurements in Andenes 2021, compared with simultaneous measurements of total aerosol surface area. The orange dots in the bottom left plot show the the average values over the INP sampling period, which are used for relationship estimates between the temperature of 50 % activated INPs in air and the other variables in the bottom right plot.

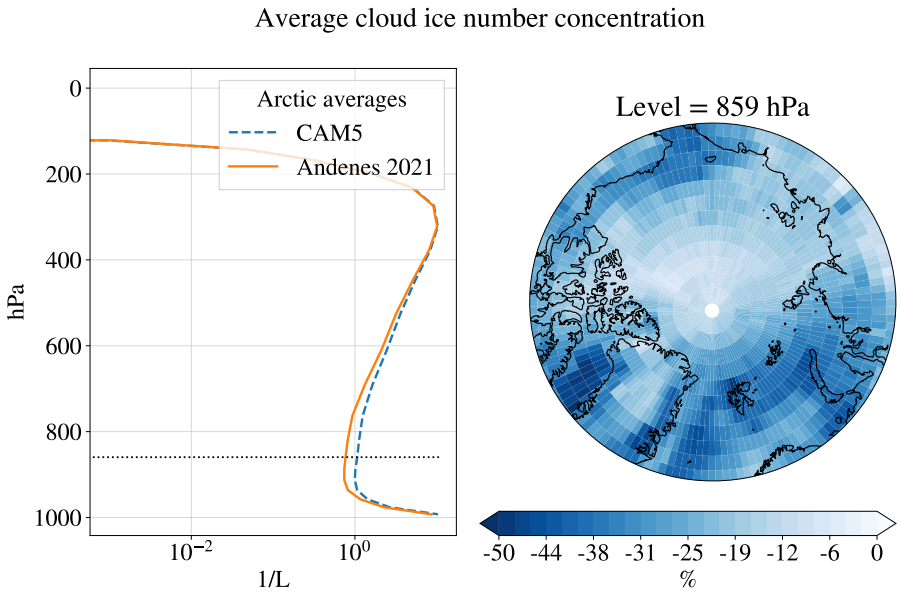

(a)

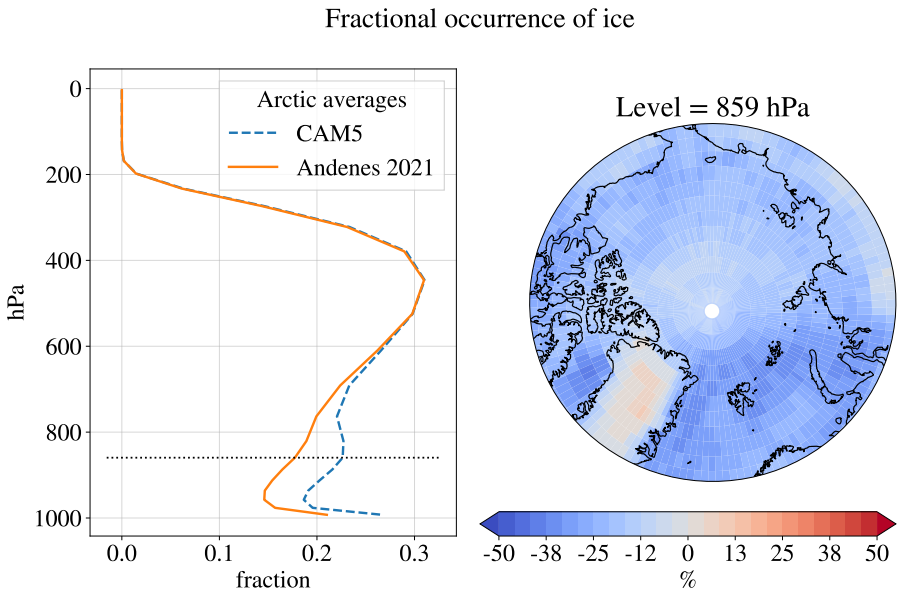

(b)

Figure A.2: The average cloud ice number concentration (a) and fractional occurence of ice (b) for "CAM5" and "Andenes 2021", averaged over the period 2007-04-15 to 2010-03-15. Left: the average values over all latitudes above 66.5°N for height levels in hybrid sigma pressure coordinates (midpoint). Right: the relative change from "CAM5" to "Andenes 2021" at pressure level 859 hPa. The level is marked with a black dotted line in the left plot.

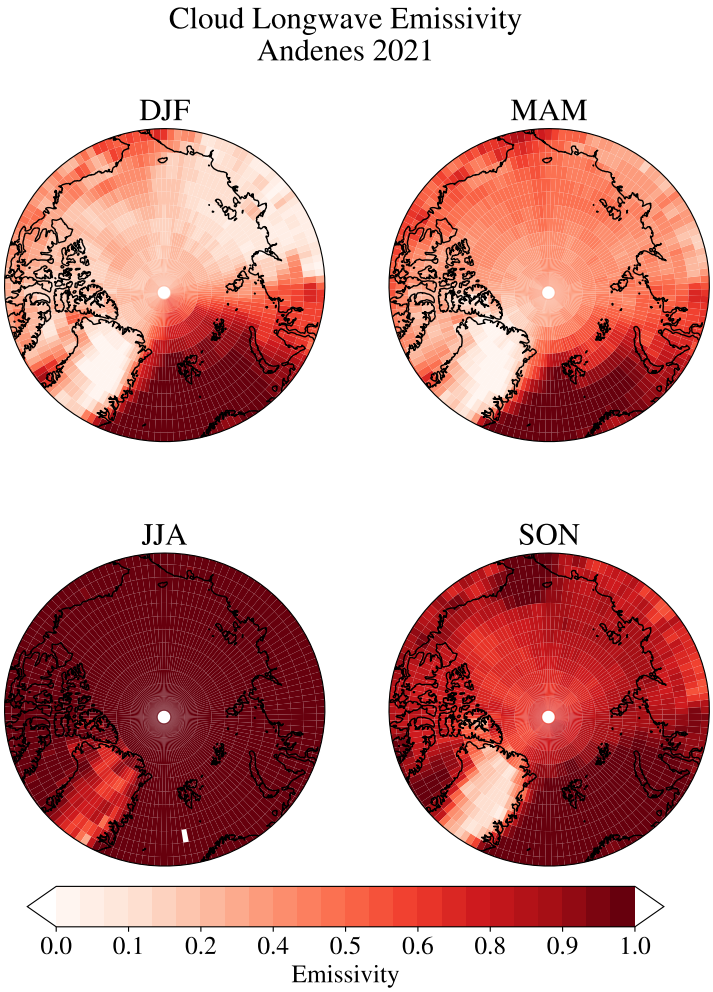

Figure A.3: The seasonal estimated cloud longwave emissivity in "Andenes 2021", averaged over the period 2007-04-15 to 2010-03-15.

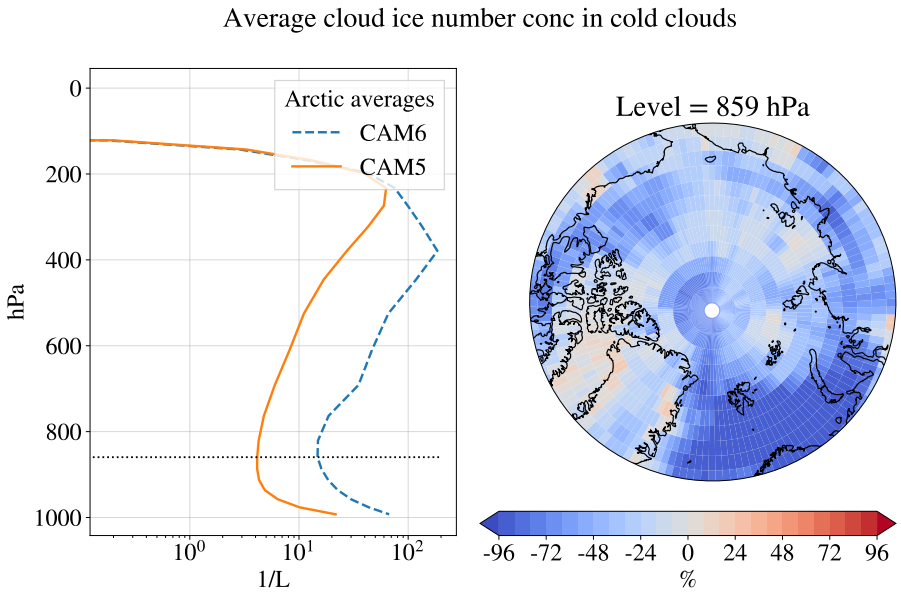

(a)

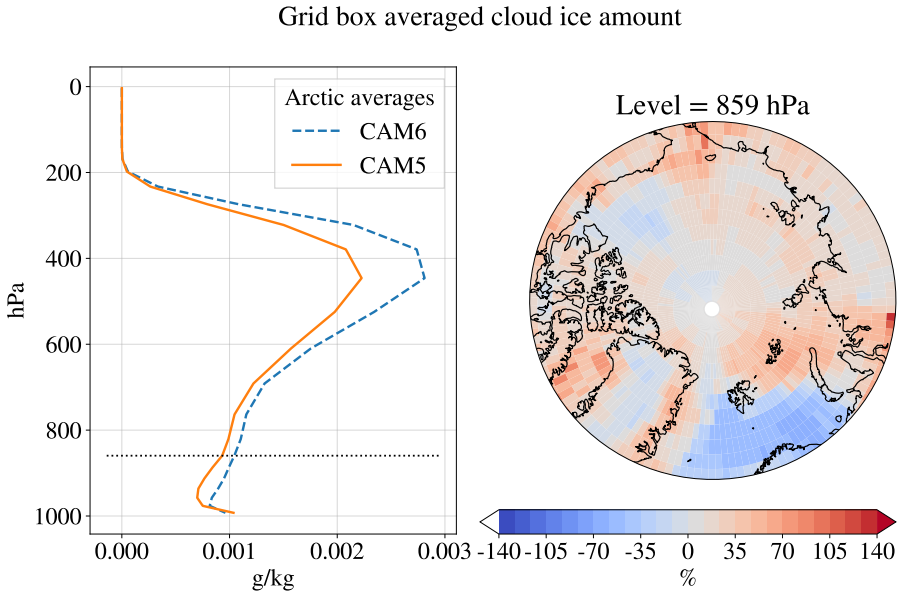

(b)

Figure A.4: The average cloud ice number concentration in cold clouds (a) and grid box averaged cloud ice amount (b) for "CAM6" and "CAM5", averaged over the period 2007-04-15 to 2010-03-15. Left: the average values over all latitudes above 66.5°N for height levels in hybrid sigma pressure coordinates (midpoint). Right: the relative change from "CAM6" to "CAM5" at pressure level 859 hPa. The level is marked with a black dotted line in the left plot.

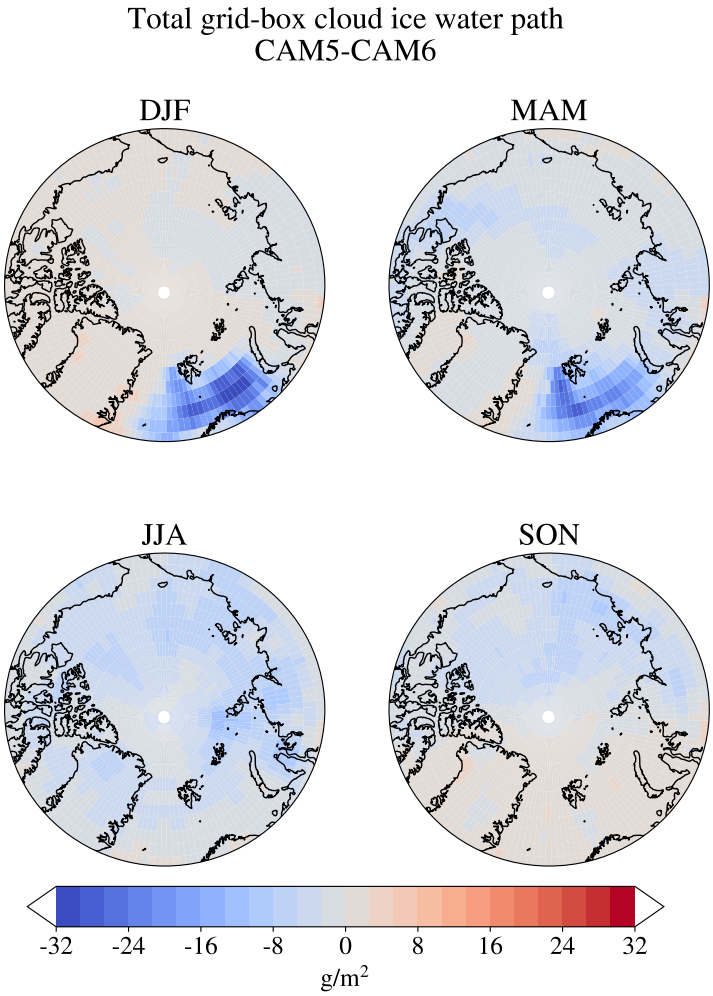

Figure A.5: The seasonal change in total grid-box cloud ice water path between "CAM5" and "CAM6", averaged over the period 2007-04-15 to 2010-03-15. Negative values correspond to lower cloud ice water path in "CAM5" compared to "CAM6".

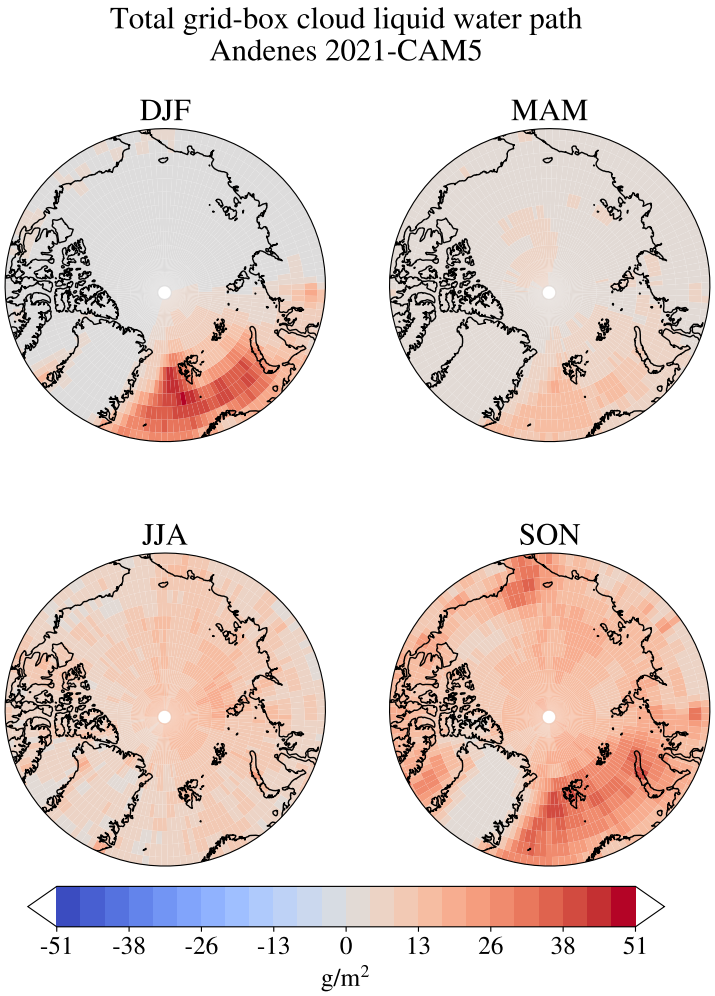

Figure A.6: The seasonal change in total grid-box cloud liquid water path between "CAM5" and "CAM6", averaged over the period 2007-04-15 to 2010-03-15. Positive values correspond to higher cloud ice water path in "CAM5" compared to "CAM6".

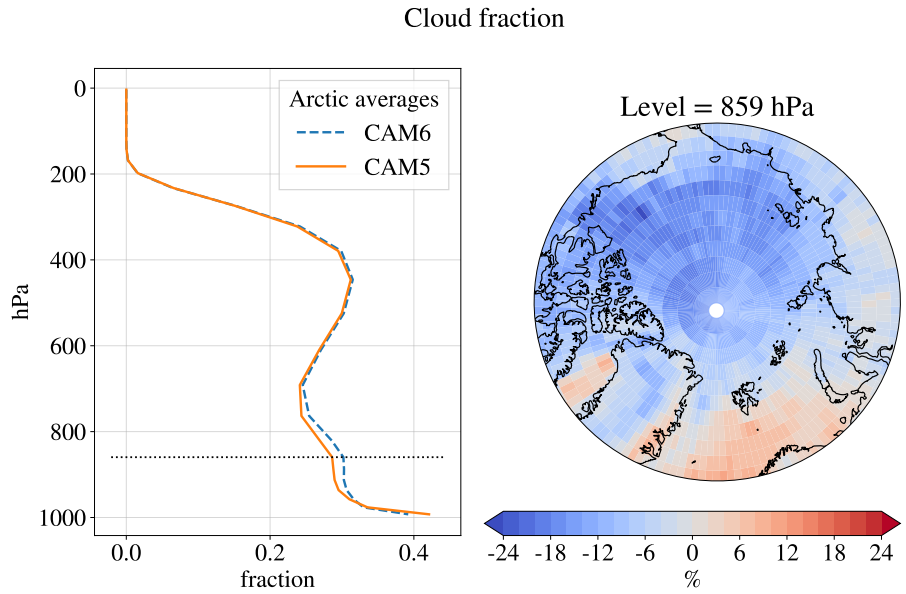

Figure A.7: The cloud fraction for "CAM6" and "CAM5", averaged over the period 2007-04-15 to 2010-03-15. Left: the average values over all latitudes above 66.5°N for height levels in hybrid sigma pressure coordinates (midpoint). Right: the relative change from "CAM6" to "CAM5" at pressure level 859 hPa. The level is marked with a black dotted line in the left plot.

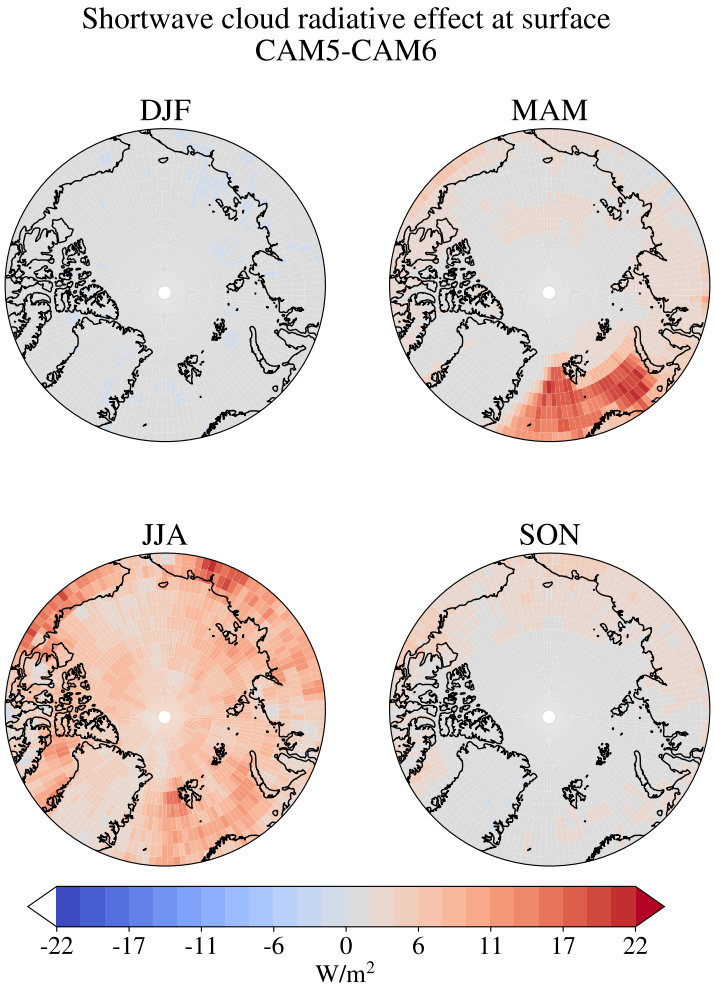

Figure A.8: The seasonal change in shortwave cloud raditative effect at the surface between "CAM5" and "CAM6", averaged over the period 2007-04-15 to 2010-03-15. Positive values correspond to more incoming solar radiation due to clouds in "CAM5" compared to "CAM6".

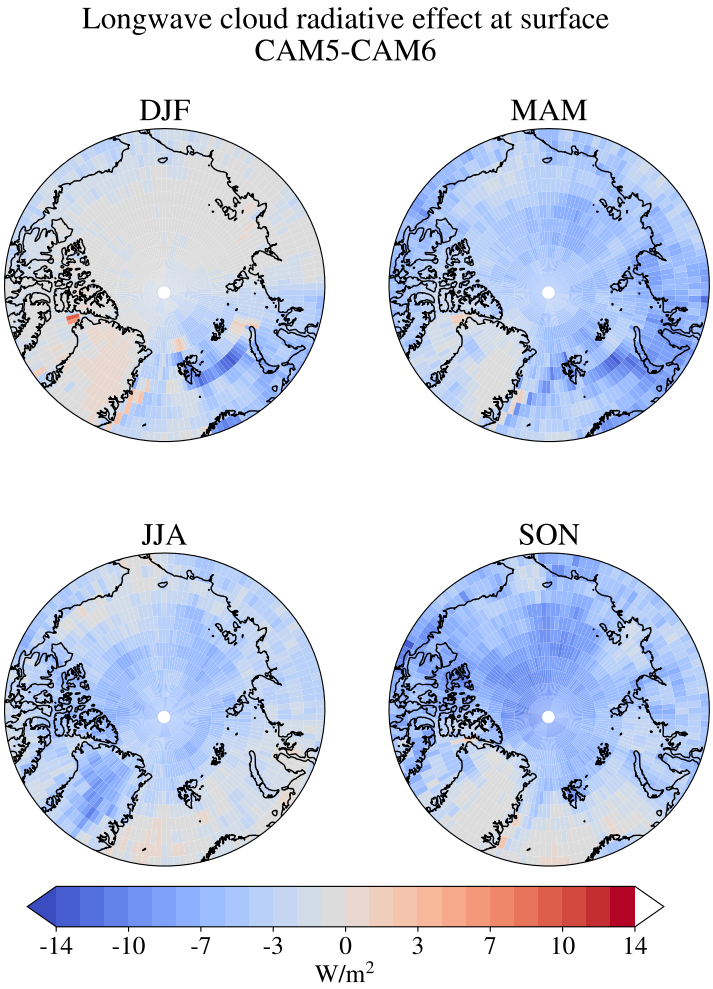

Figure A.9: The seasonal change in longwave cloud radiative effect at the surface between "CAM5" and "CAM6", averaged over the period 2007-04-15 to 2010-03-15. Negative values correspond to more outgoing longwave radiation due to clouds in "CAM5" compared to "CAM6".

APPENDIX B

Data and Code Accesibility

This master thesis can be found as a Research Object on https://w3id.org/ro-id/8e232746-8c6f-4e55-bc9a-4db222e86ca1.

B.1 Observational Data and Code

All observational data produced in this thesis is stored in the Norwegian National Infrastructure for Research Data (NIRD) Research Archive, and be provided upon request. The archive includes freezing temperature data for all Coriolis and sea water samples, as well as aerosol measurements, inlet temperature data and measured total organic carbon (TOC).

The pressure and wind data used in this thesis was accessed through the Frost API, which provides free access to MET Norway's archive of historical weather and climate data. Description of how to access the data can be found at https://github.com/franzihe/metNo_obs_data, courtesy of Franziska Hellmuth (University of Oslo; Institute of Geosciences; Department of Meteorology and Oceanography).

The scripts for postprocessing of observations can be found at https://github.com/astridbg/master/tree/main/scripts/observations/PostProcessing. The scripts for data analysis and visualisation of observational data can be found at https://github.com/astridbg/master/tree/main/scripts/observations.

B.2 Model Data and Code

The data from the NorESM2 model runs produced in this thesis is stored in NIRD Research Archive and can be provided upon request. The CALIOP L2 data used to derive SLF metrics can be freely downloaded at https://search.earthdata.nasa.gov/, and was provided to me by Stefan Hofer (University of Oslo; Institute of Geosciences; Department of Meteorology and Oceanography).

Information about the specific versions of the different model components I have used can be found at https://github.com/astridbg/master/blob/main/noresm/Externals.cfg. The sourcecode modifications and given namelist

options for the different model experiements can accessed at the following places:

- **CAM6:**
  https://github.com/astridbg/master/tree/main/noresm/NF2000climo_f19_tn14_def_20210126
- **CAM5:**
  https://github.com/astridbg/master/tree/main/noresm/NF2000climo_f19_tn14_meyers92_20220210
- **Andenes 2021:**
  https://github.com/astridbg/master/tree/main/noresm/NF2000climo_f19_tn14_andenes21_20220222

The script for postprocessing of the modelling data can be found at https://github.com/astridbg/master/tree/main/scripts/model/PostProcessing.py. The scripts for spatial and temporal averages, as well as model data visualisation can be found at https://github.com/astridbg/master/tree/main/scripts/model

Bibliography

Abbatt, J. P. D., Benz, S., Cziczo, D. J., Kanji, Z., Lohmann, U. and Möhler, O. (2006). 'Solid ammonium sulfate aerosols as ice nuclei: A pathway for cirrus cloud formation'. In: *Science* vol. 313, pp. 1770–1773.

Ansmann, A. et al. (2008). 'Influence of Saharan dust on cloud glaciation in southern Morocco during the Saharan Mineral Dust Experiment'. In: *Journal of Geophysical Research: Atmospheres* vol. 113, no. D4. eprint: https://agupubs.onlinelibrary.wiley.com/doi/pdf/10.1029/2007JD008785.

Auer, A. H., Veal, D. L. and Marwitz, J. D. (1969). 'Observations of Ice Crystal and Ice Nuclei Concentrations in Stable Cap Clouds'. In: *Journal of Atmospheric Sciences* vol. 26, no. 6, pp. 1342–1343.

Beall, C. M., Lucero, D., Hill, T. C., DeMott, P. J., Stokes, M. D. and Prather, K. A. (2020). 'Best practices for precipitation sample storage for offline studies of ice nucleation in marine and coastal environments'. In: *Atmospheric Measurement Techniques* vol. 13, no. 12, pp. 6473–6486.

Bentsen, M. (2020). 'Bergen Layered Ocean Model (BLOM): Description and evaluation of global ocean–sea-ice experiments'. In: *Geosci. Model. Dev. Discuss., in preparation.*

Bentsen, M. et al. (2013). 'The Norwegian Earth System Model, NorESM1-M – Part 1: Description and basic evaluation of the physical climate'. In: *Geoscientific Model Development* vol. 6, no. 3, pp. 687–720.

Bergeron, T. (1935). *On the physics of clouds and precipitation.* Proces Verbaux de l'Association de Météorologie, International Union of Geodesy and Geophysics, 156–178.

Bigg, E. K. (1953). 'The formation of atmospheric ice crystals by the freezing of droplets'. In: *Quarterly Journal of the Royal Meteorological Society* vol. 79, no. 342, pp. 510–519.

Bjordal, J., Storelvmo, T., Alterskjær, K. and Carlsen, T. (Nov. 2020). 'Equilibrium climate sensitivity above 5 °C plausible due to state-dependent cloud feedback'. In: *Nature Geoscience* vol. 13, no. 11, pp. 718–721.

Boer, G., Morrison, H., Shupe, M. and Hildner, R. (Jan. 2011). 'Evidence of liquid dependent ice nucleation in high-latitude stratiform clouds from surface remote sensors'. In: *Geophysical Research Letters* vol. 38.

Borduas-Dedekind, N., Ossola, R., David, R. O., Boynton, L. S., Weichlinger, V., Kanji, Z. A. and McNeill, K. (2019). 'Photomineralization mechanism changes the ability of dissolved organic matter to activate cloud droplets

and to nucleate ice crystals'. In: *Atmospheric Chemistry and Physics* vol. 19, no. 19, pp. 12397–12412.

Bruno, O., Hoose, C., Storelvmo, T., Coopman, Q. and Stengel, M. (Jan. 2021). 'Exploring the Cloud Top Phase Partitioning in Different Cloud Types Using Active and Passive Satellite Sensors'. In: *Geophysical Research Letters* vol. 48.

Burrows, S. M., Hoose, C., Pöschl, U. and Lawrence, M. G. (2013). 'Ice nuclei in marine air: biogenic particles or dust?' In: *Atmospheric Chemistry and Physics* vol. 13, no. 1, pp. 245–267.

Carlsen, T. and David, R. O. (2022). 'Spaceborne evidence that ice-nucleating particles influence cloud phase'. In: *Earth and Space Science Open Archive*, p. 17.

Creamean, J. M. et al. (2019). 'Ice Nucleating Particles Carried From Below a Phytoplankton Bloom to the Arctic Atmosphere'. In: *Geophysical Research Letters* vol. 46, no. 14, pp. 8572–8581. eprint: https://agupubs.onlinelibrary.wiley.com/doi/pdf/10.1029/2019GL083039.

Danabasoglu, G., Lamarque, J.-F., Bacmeister, J., Bailey, D. A., DuVivier, A. K., Edwards, J. and al., et (2020). 'The Community Earth System Model Version 2 (CESM2)'. In: *Journal of Advances in Modeling Earth Systems* vol. 12, e2019MS001916, pp. 2209–2221.

David, R. O. et al. (2019a). 'Development of the DRoplet Ice Nuclei Counter Zurich (DRINCZ): validation and application to field-collected snow samples'. In: *Atmospheric Measurement Techniques* vol. 12, no. 12, pp. 6865–6888.

David, R. O., Marcolli, C., Fahrni, J., Qiu, Y., Sirkin, Y. A. P., Molinero, V., Mahrt, F., Brühwiler, D., Lohmann, U. and Kanji, Z. A. (2019b). 'Pore condensation and freezing is responsible for ice formation below water saturation for porous particles'. In: *Proceedings of the National Academy of Sciences* vol. 116, no. 17, pp. 8184–8189. eprint: https://www.pnas.org/doi/pdf/10.1073/pnas.1813647116.

Dee, D. P. et al. (2011). 'The ERA-Interim reanalysis: configuration and performance of the data assimilation system'. In: *Quarterly Journal of the Royal Meteorological Society* vol. 137, no. 656, pp. 553–597. eprint: https://rmets.onlinelibrary.wiley.com/doi/pdf/10.1002/qj.828.

DeMott, P. J., Prenni, A. J., Liu, X., Kreidenweis, S. M., Petters, M. D., Twohy, C. H., Richardson, M. S., Eidhammer, T. and Rogers, D. C. (2010). 'Predicting global atmospheric ice nuclei distributions and their impacts on climate'. In: *Proceedings of the National Academy of Sciences* vol. 107, no. 25, pp. 11217–11222. eprint: https://www.pnas.org/doi/pdf/10.1073/pnas.0910818107.

DeMott, P. J. et al. (2016). 'Sea spray aerosol as a unique source of ice nucleating particles'. In: *Proceedings of the National Academy of Sciences* vol. 113, no. 21, pp. 5797–5803. eprint: https://www.pnas.org/doi/pdf/10.1073/pnas.1514034112.

Després, V. R. (2012). 'Primary biological aerosol particles in the atmosphere: A review'. In: *Tellus* vol. 64B.

Eyring, V., Bony, S., Meehl, G. A., Senior, C. A., Stevens, B., Stouffer, R. J. and Taylor, K. E. (2016). 'Overview of the Coupled Model Intercomparison Project Phase 6 (CMIP6) experimental design and organization'. In: *Geoscientific Model Development* vol. 9, no. 5, pp. 1937–1958.

Field, P. R. et al. (2017). 'Secondary Ice Production: Current State of the Science and Recommendations for the Future'. In: *Meteorological Monographs* vol. 58, pp. 7.1–7.20.

Findeisen, W. (1938). 'Kolloid-meteorologische Vorgänge bei Neiderschlagsbildung.' In: *Meteor. Z* vol. 55, pp. 121–133.

Forster, P. et al. (2021). 'The Earth's Energy Budget, Climate Feedbacks, and Climate Sensitivity'. In: *Climate Change 2021: The Physical Science Basis. Contribution of Working Group I to the Sixth Assessment Report of the Intergovernmental Panel on Climate Change*. Ed. by Masson-Delmotte, V. et al. Cambridge University Press.

Fröhlich-Nowoisky, J., Hill, T. C. J., Pummer, B. G., Franc, G. D. and Pöschl, U. (2015). 'Ice nucleation activity in the widespread soil fungus Mortierella alpina'. In: *Biogeosciences* vol. 12, pp. 1057–1071.

Griesche, H. J., Ohneiser, K., Seifert, P., Radenz, M., Engelmann, R. and Ansmann, A. (2021). 'Contrasting ice formation in Arctic clouds: surface-coupled vs. surface-decoupled clouds'. In: *Atmospheric Chemistry and Physics* vol. 21, no. 13, pp. 10357–10374.

Hallett, J. and Mossop, S. (1974). 'Production of secondary ice particles during the riming process'. In: *Nature* vol. 249, pp. 26–28.

Hofer, S. (2022). Personal communication.

Hoose, C. and Möhler, O. (2012). 'Heterogeneous ice nucleation on atmospheric aerosols: a review of results from laboratory experiments'. In: *Atmospheric Chemistry and Physics* vol. 12, no. 20, pp. 9817–9854.

Hoose, C., Kristjánsson, J. E., Chen, J.-P. and Hazra, A. (2010). 'A Classical-Theory-Based Parameterization of Heterogeneous Ice Nucleation by Mineral Dust, Soot, and Biological Particles in a Global Climate Model'. In: *Journal of the Atmospheric Sciences* vol. 67, no. 8, pp. 2483–2503.

Huang, W. T. K., Ickes, L., Tegen, I., Rinaldi, M., Ceburnis, D. and Lohmann, U. (2018). 'Global relevance of marine organic aerosol as ice nucleating particles'. In: *Atmospheric Chemistry and Physics* vol. 18, no. 15, pp. 11423–11445.

Hunke, E., Lipscomb, W., Jones, P., Turner, A., Jeffery, N. and Elliott, S. (2015). *CICE: the Los Alamos Sea Ice Model Documentation and Software User's Manual Version 5.1*. Los Alamos National Laboratory, Los Alamos, New Mexico, USA.

Hurrell, J. W. et al. (2013). 'The Community Earth System Model: A Framework for Collaborative Research'. In: *Bulletin of the American Meteorological Society* vol. 94, no. 9, pp. 1339–1360.

Inoue, J., Tobo, Y., Taketani, F. and Sato, K. (2021). 'Oceanic Supply of Ice-Nucleating Particles and Its Effect on Ice Cloud Formation: A Case Study in the Arctic Ocean During a Cold-Air Outbreak in Early Winter'. In: *Geophysical Research Letters* vol. 48, no. 16. e2021GL094646 2021GL094646, e2021GL094646. eprint: https://agupubs.onlinelibrary.wiley.com/doi/pdf/10.1029/2021GL094646.

Irish, V. E. et al. (2017). 'Ice-nucleating particles in Canadian Arctic sea-surface microlayer and bulk seawater'. In: *Atmospheric Chemistry and Physics* vol. 17, no. 17, pp. 10583–10595.

Irish, V. E. et al. (2019). 'Revisiting properties and concentrations of ice-nucleating particles in the sea surface microlayer and bulk seawater in the Canadian Arctic during summer'. In: *Atmospheric Chemistry and Physics* vol. 19, no. 11, pp. 7775–7787.

Iversen, T. et al. (2013). 'The Norwegian Earth System Model, NorESM1-M – Part 2: Climate response and scenario projections'. In: *Geoscientific Model Development* vol. 6, no. 2, pp. 389–415.

Kanji, Z. A., Ladino, L. A., Wex, H., Boose, Y., Burkert-Kohn, M., Cziczo, D. J. and Krämer, M. (2017). 'Overview of Ice Nucleating Particles'. In: *Meteorological Monographs* vol. 58, pp. 1.1–1.33.

Kartverket (2022). http://norgeskart.no. Accessed: 2022-04-26.

Kay, J. E. and Gettelman, A. (2009). 'Cloud influence on and response to seasonal Arctic sea ice loss'. In: *Journal of Geophysical Research: Atmospheres* vol. 114, no. D18. eprint: https://agupubs.onlinelibrary.wiley.com/doi/pdf/10.1029/2009JD011773.

Kirkevåg, A. et al. (2013). 'Aerosol–climate interactions in the Norwegian Earth System Model – NorESM1-M'. In: *Geoscientific Model Development* vol. 6, no. 1, pp. 207–244.

Kirkevåg, A. et al. (2018). 'A production-tagged aerosol module for Earth system models, OsloAero5.3 – extensions and updates for CAM5.3-Oslo'. In: *Geoscientific Model Development* vol. 11, no. 10, pp. 3945–3982.

Korolev, A. and Leisner, T. (2020). 'Review of experimental studies of secondary ice production'. In: *Atmospheric Chemistry and Physics* vol. 20, no. 20, pp. 11767–11797.

Lamb, D. and Verlinde, J. (2011). *Physics and Chemistry of Clouds*. Cambridge University Press.

Lawrence, D. M. et al. (2019). 'The Community Land Model Version 5: Description of New Features, Benchmarking, and Impact of Forcing Uncertainty'. In: *Journal of Advances in Modeling Earth Systems* vol. 11, no. 12, pp. 4245–4287.

Lenton, T. (2016). *Earth System Science, A Very Short Introduction*. Oxford University Press.

Li, G., Wieder, J., Pasquier, J. T., Henneberger, J. and Kanji, Z. A. (2022). 'Predicting atmospheric background number concentration of ice nucleating particles in the Arctic'. In: *Atmospheric Chemistry and Physics Discussions* vol. 2022, pp. 1–27.

Marcolli, C. (2014). 'Deposition nucleation viewed as homogeneous or immersion freezing in pores and cavities'. In: *Atmospheric Chemistry and Physics* vol. 14, no. 4, pp. 2071–2104.

Marcolli, C. (Nov. 2017). 'Ice nucleation triggered by negative pressure'. In: *Scientific Reports* vol. 7, no. 1, p. 16634.

Marinou, E. et al. (2019). 'Retrieval of ice-nucleating particle concentrations from lidar observations and comparison with UAV in situ measurements'. In: *Atmospheric Chemistry and Physics* vol. 19, no. 17, pp. 11315–11342.

McCluskey, C. S., DeMott, P. J., Ma, P.-L. and Burrows, S. M. (2019). 'Numerical Representations of Marine Ice-Nucleating Particles in Remote Marine Environments Evaluated Against Observations'. In: *Geophysical Research Letters* vol. 46, no. 13, pp. 7838–7847. eprint: https://agupubs.onlinelibrary.wiley.com/doi/pdf/10.1029/2018GL081861.

McCluskey, C. S. et al. (2017). 'A Dynamic Link between Ice Nucleating Particles Released in Nascent Sea Spray Aerosol and Oceanic Biological Activity during Two Mesocosm Experiments'. In: *Journal of the Atmospheric Sciences* vol. 74, no. 1, pp. 151–166.

McCluskey, C. S. et al. (2018). 'Marine and Terrestrial Organic Ice-Nucleating Particles in Pristine Marine to Continentally Influenced Northeast Atlantic Air Masses'. In: *Journal of Geophysical Research: Atmospheres* vol. 123, no. 11, pp. 6196–6212. eprint: https://agupubs.onlinelibrary.wiley.com/doi/pdf/10.1029/2017JD028033.

Meyers, M. P., DeMott, P. J. and Cotton, W. R. (1992). 'New Primary Ice-Nucleation Parameterizations in an Explicit Cloud Model'. In: *Journal of Applied Meteorology and Climatology* vol. 31, no. 7, pp. 708–721.

Miller, A. J., Brennan, K. P., Mignani, C., Wieder, J., David, R. O. and Borduas-Dedekind, N. (2021). 'Development of the drop Freezing Ice Nuclei Counter (FINC), intercomparison of droplet freezing techniques, and use of soluble lignin as an atmospheric ice nucleation standard'. In: *Atmospheric Measurement Techniques* vol. 14, no. 4, pp. 3131–3151.

Mossop, S. (1970). 'Concentrations of ice crystals in clouds'. In: *Bull. Amer. Meteor. Soc.* vol. 51, pp. 474–479.

Murray, B. J., Carslaw, K. S. and Field, P. R. (2021). 'Opinion: Cloud-phase climate feedback and the importance of ice-nucleating particles'. In: *Atmospheric Chemistry and Physics* vol. 21, no. 2, pp. 665–679.

Murray, B. J., O'Sullivan, D., Atkinson, J. D. and Webb, M. E. (2012). 'Ice nucleation by particles immersed in supercooled cloud droplets'. In: *Chem. Soc. Rev.* vol. 41 (19), pp. 6519–6554.

Niehaus, J. and Cantrell, W. (2015). 'Contact freezing of water by salts'. In: *J. Phys. Chem. Lett.* vol. 6, pp. 3490–3495.

Otto, F. E. L. (2012). 'Modelling the earth's climate - an epistemic perspective'. PhD thesis.

Pithan, F. and Mauritsen, T. (Mar. 2014). 'Arctic amplification dominated by temperature feedbacks in contemporary climate models'. In: *Nature Geoscience* vol. 7, no. 3, pp. 181–184.

Prenni, A. J., Harrington, J. Y., Tjernström, M., DeMott, P. J., Avramov, A., Long, C. N., Kreidenweis, S. M., Olsson, P. Q. and Verlinde, J. (2007). 'Can Ice-Nucleating Aerosols Affect Arctic Seasonal Climate?' In: *Bulletin of the American Meteorological Society* vol. 88, no. 4, pp. 541–550.

Pummer, B. G., Bauer, H., Bernardi, J., Bleicher, S. and Grothe, H. (2012). 'Suspendable macromolecules are responsible for ice nucleation activity of birch and conifer pollen'. In: *Atmos. Chem. Phys.* vol. 12, pp. 2541–2550.

Rantanen, M., Karpechko, A., Lipponen, A., Nordling, K., Hyvärinen, O., Ruosteenoja, K., Vihma, T. and Laaksonen, A. (2021). 'The Arctic has warmed four times faster than the globe since 1980'. In: PREPRINT (Version 1) available at Research Square.

Schrod, J. et al. (2017). 'Ice nucleating particles over the Eastern Mediterranean measured by unmanned aircraft systems'. In: *Atmospheric Chemistry and Physics* vol. 17, no. 7, pp. 4817–4835.

Seland, Ø. et al. (2020a). 'Overview of the Norwegian Earth System Model (NorESM2) and key climate response of CMIP6 DECK, historical, and scenario simulations'. In: *Geoscientific Model Development* vol. 13, no. 12, pp. 6165–6200.

Seland, Ø. et al. (Oct. 2020b). *NorESM2 source code as used for CMIP6 simulations (includes additional experimental setups, extended model documentation, automated inputdata download, restructuring of BLOM/iHAMOCC input data)*. Version 2.0.2.

Shaw, J., McGraw, Z., Bruno, O., Storelvmo, T. and Hofer, S. (2022). 'Using Satellite Observations to Evaluate Model Microphysical Representation of Arctic Mixed-Phase Clouds'. In: *Geophysical Research Letters* vol. 49, no. 3. e2021GL096191 2021GL096191, e2021GL096191. eprint: https://agupubs.onlinelibrary.wiley.com/doi/pdf/10.1029/2021GL096191.

Stephens, G. L. (1978). 'Radiation Profiles in Extended Water Clouds. II: Parameterization Schemes'. In: *Journal of Atmospheric Sciences* vol. 35, no. 11, pp. 2123–2132.

Stephens, G. L. (2003). *Radiative Properties of Clouds.* https://reef.atmos.colostate.edu/~odell/AT622/stephens_notes/. Lecture notes ($AT622_section16$) : $ColoradoStateUniverstiy, Departmentof AtmosphericSciences$.

Storelvmo, T. and Tan, I. (Apr. 2015). 'The Wegener-Bergeron-Findeisen process - Its discovery and vital importance for weather and climate'. In: *Meteorologische Zeitschrift* vol. 24, pp. 455–461.

Tan, I. and Storelvmo, T. (2019). 'Evidence of Strong Contributions From Mixed-Phase Clouds to Arctic Climate Change'. In: *Geophysical Research Letters* vol. 46, no. 5, pp. 2894–2902. eprint: https://agupubs.onlinelibrary.wiley.com/doi/pdf/10.1029/2018GL081871.

Tan, I., Storelvmo, T. and Zelinka, M. D. (2016). 'Observational constraints on mixed-phase clouds imply higher climate sensitivity'. In: *Science* vol. 352, no. 6282, pp. 224–227. eprint: https://www.science.org/doi/pdf/10.1126/science.aad5300.

Tjiputra, J. F. et al. (2020). 'Ocean biogeochemistry in the Norwegian Earth System Model version 2 (NorESM2)'. In: *Geoscientific Model Development* vol. 13, no. 5, pp. 2393–2431.

Tobo, Y. et al. (Apr. 2019). 'Glacially sourced dust as a potentially significant source of ice nucleating particles'. In: *Nature Geoscience* vol. 12, no. 4, pp. 253–258.

Toniazzo, T., Bentsen, M., Craig, C., Eaton, B. E., Edwards, J., Goldhaber, S., Jablonowski, C. and Lauritzen, P. H. (2020). 'Enforcing conservation of axial angular momentum in the atmospheric general circulation model CAM6'. In: *Geoscientific Model Development* vol. 13, no. 2, pp. 685–705.

Twomey, S. (1974). 'Pollution and the planetary albedo'. In: *Atmospheric Environment (1967)* vol. 8, no. 12, pp. 1251–1256.

Vali, G., DeMott, P. J., Möhler, O. and Whale, T. F. (2015). 'Technical Note: A proposal for ice nucleation terminology'. In: *Atmospheric Chemistry and Physics* vol. 15, no. 18, pp. 10263–10270.

Vali, G. (1971). 'Quantitative Evaluation of Experimental Results an the Heterogeneous Freezing Nucleation of Supercooled Liquids'. In: *Journal of the Atmospheric Sciences* vol. 28, no. 3, pp. 402–409.

Vergara-Temprado, J. et al. (2017). 'Contribution of feldspar and marine organic aerosols to global ice nucleating particle concentrations'. In: *Atmospheric Chemistry and Physics* vol. 17, no. 5, pp. 3637–3658.

Wadhams, P. (2000). *Ice in the Ocean.* CRC Press.

Wegener, A. (1911). *Thermodynamik der Atmosphäre.* Leipzig, 311.p.

Westbrook, C. and Illingworth, A. (2013). 'The formation of ice in a long-lived supercooled layer cloud'. In: *Q.J.R. Meteorol. Soc* vol. 139, pp. 2209–2221.

Wex, H. et al. (2019). 'Annual variability of ice-nucleating particle concentrations at different Arctic locations'. In: *Atmospheric Chemistry and Physics* vol. 19, no. 7, pp. 5293–5311.

Wilson, T. W. et al. (Sept. 2015). 'A marine biogenic source of atmospheric ice-nucleating particles'. In: *Nature* vol. 525, no. 7568, pp. 234–238.

Winker, D. M., Vaughan, M. A., Omar, A., Hu, Y., Powell, K. A., Liu, Z., Hunt, W. H. and Young, S. A. (2009). 'Overview of the CALIPSO Mission and CALIOP Data Processing Algorithms'. In: *Journal of Atmospheric and Oceanic Technology* vol. 26, no. 11, pp. 2310–2323.

Young, K. C. (1974). 'The Role of Contact Nucleation in Ice Phase Initiation in Clouds'. In: *Journal of Atmospheric Sciences* vol. 31, no. 3, pp. 768–776.

Yun, Y. and Penner, J. E. (2013). 'An evaluation of the potential radiative forcing and climatic impact of marine organic aerosols as heterogeneous ice nuclei'. In: *Geophysical Research Letters* vol. 40, no. 15, pp. 4121–4126. eprint: https://agupubs.onlinelibrary.wiley.com/doi/pdf/10.1002/grl.50794.

Zelinka, M. D., Myers, T. A., McCoy, D. T., Po-Chedley, S., Caldwell, P. M., Ceppi, P., Klein, S. A. and Taylor, K. E. (2020). 'Causes of Higher Climate Sensitivity in CMIP6 Models'. In: *Geophysical Research Letters* vol. 47, no. 1. e2019GL085782 10.1029/2019GL085782, e2019GL085782. eprint: https://agupubs.onlinelibrary.wiley.com/doi/pdf/10.1029/2019GL085782.

Zhang, T., Stamnes, K. and Bowling, S. A. (1996). 'Impact of Clouds on Surface Radiative Fluxes and Snowmelt in the Arctic and Subarctic'. In: *Journal of Climate* vol. 9, no. 9, pp. 2110–2123.

Zhao, X., Liu, X., Burrows, S. M. and Shi, Y. (2021). 'Effects of marine organic aerosols as sources of immersion-mode ice-nucleating particles on high-latitude mixed-phase clouds'. In: *Atmospheric Chemistry and Physics* vol. 21, no. 4, pp. 2305–2327.